Villin Controls the Formation and Enlargement of Punctate Actin Foci in Pollen Tubes

Zhao, Wanying ; Qu, Xiaolu; Zhuang, Yuhui; Wang, Ludi; Bosch, Maurice; Franklin-Tong, Vernonica E.; Huang, Shanjin

Published in:
Journal of Cell Science

DOI:
10.1242/jcs.237404

Publication date:
2020

Citation for published version (APA):
Zhao, W., Qu, X., Zhuang, Y., Wang, L., Bosch, M., Franklin-Tong, V. E., & Huang, S. (2020). Villin Controls the Formation and Enlargement of Punctate Actin Foci in Pollen Tubes. *Journal of Cell Science*, *133*(6), [237404]. https://doi.org/10.1242/jcs.237404

Villin Controls the Formation and Enlargement of Punctate Actin Foci in Pollen Tubes

Wanying Zhao[1,#], Xiaolu Qu[1,6,#], Yuhui Zhuang[1,#], Ludi Wang[5], Maurice Bosch[5], Vernonica E Franklin-Tong[4], Yongbiao Xue[2,3] and Shanjin Huang[1,*]

[1]Center for Plant Biology, School of Life Sciences, Tsinghua University, Beijing, 100084, China

[2]State Key Laboratory of Molecular Developmental Biology, Institute of Genetics and Developmental Biology, Chinese Academy of Sciences, Beijing, 100101, China.

[3]Beijing Institute of Genomics, Chinese Academy of Sciences, Beijing, 100101, China.

[4]School of Biosciences, College of Life and Environmental Sciences, University of Birmingham, Edgbaston, Birmingham, B15 2TT, UK

[5]Institute of Biological, Environmental and Rural Sciences (IBERS), Aberystwyth University, Plas Gogerddan, Aberystwyth, SY23 3EE, UK

[6]Key Laboratory of Horticultural Plant Biology (Ministry of Education), College of Horticulture and Forestry Sciences, Huazhong Agricultural University, Wuhan, China

[#]Contributed equally to this work

[*]Correspondence should be addressed to:

Dr. Shanjin Huang

Center for Plant Biology, School of Life Sciences, Tsinghua University, 100084 Beijing, China

E-mail: sjhuang@tsinghua.edu.cn

Tel: 86-10-62781946

Key words: actin depolymerization, pollen tube, villin, actin filament severing, actin monomer dissociation, actin foci, self-incompatibility response

JCS Advance Online Article. Posted on 12 February 2020

ABSTRACT

Self-incompatibility (SI) in *Papaver rhoeas* triggers dramatic actin alterations in pollen. However, how actin alterations in SI pollen tubes are mechanistically achieved remains largely unexplored. Here we have used treatment with the calcium ionophore A23187 to mimic the SI-induced elevation in cytosolic Ca^{2+} and trigger the formation of the distinctive F-actin foci. Live-cell imaging reveals that this remodeling involves F-actin fragmentation and depolymerization, accompanied by the rapid formation of punctate actin foci and subsequent increase in their size. We establish that actin foci are generated and enlarged from crosslinking of fragmented actin filament structures. Moreover, we show that villins associate with actin structures and are involved in this actin reorganization process. Notably, we demonstrate that *Arabidopsis* villin5 promotes actin depolymerization and formation of actin foci by fragmenting actin filaments, and controlling the enlargement of actin foci *via* bundling actin filaments. Our study thus uncovers important, novel insights about the molecular players and mechanisms involved in forming the distinctive actin foci in pollen tubes.

INTRODUCTION

The actin cytoskeleton is a complex dynamic network that undergoes rapid assembly and disassembly in response to various internal and external cues (Staiger, 2000). Well documented examples in plants include the rearrangement of the actin cytoskeleton in root hairs during Nod factor infection from *Rhizobium* bacteria (Cardenas et al., 2003; Cardenas et al., 1998), the rearrangement of the actin cytoskeleton during the cell cycle (Sano et al., 2005; Yu et al., 2006), pathogen infection (Takemoto et al., 2003), stomatal closure and opening (Eun and Lee, 1997; Gao et al., 2008; Hwang and Lee, 2001) and the dramatic depolymerization and rearrangement of the actin cytoskeleton in *Papaver rhoeas* pollen during the self-incompatibility (SI) response (Geitmann et al., 2000; Poulter et al., 2010; Snowman et al., 2002). These cellular changes are triggered by increases in cytosolic free Ca^{2+} ($[Ca^{2+}]_{cyt}$) to trigger a Ca^{2+}-dependent signaling network involving increases in pH and reactive oxygen species to trigger programmed cell death (PCD) (Thomas et al., 2006; Wang et al., 2019; Wilkins et al., 2014). However, the molecular players and mechanisms underlying the rapid and dramatic actin alterations in pollen tubes in response to SI signaling remain largely unexplored.

The pollen tube is a model cellular system to study tip growth and its regulation (Bedinger et al., 1994; Feijo et al., 2001; Hepler et al., 2001; Holdaway-Clarke and Hepler, 2003), and the actin cytoskeleton is known to play a critical role in regulating pollen tube growth (Gibbon et al., 1999; Qu et al., 2017; Vidali et al., 2001). It has been shown that Ca^{2+} signaling and the actin cytoskeleton are inherently correlated during pollen tube growth, as evidenced by the observations that both $[Ca^{2+}]$ and F-actin levels oscillate during pollen tube growth (Diao et al., 2018; Fu et al., 2001; Holdaway-Clarke and Hepler, 2003; Hwang et al., 2005). SI is a genetically controlled pollen-pistil recognition system controlled by tightly linked polymorphic *S*-determinant genes expressed in the pollen and pistil. Interaction of cognate *S*-determinants results in inhibition of incompatible pollen tube growth. In *P. rhoeas*, the *S*-determinants are PrsS

(a small secreted signalling ligand, related to cysteine rich proteins) and PrpS, a small, novel transmembrane protein (Foote et al., 1994; Wheeler et al., 2010). Cognate PrsS and PrpS interact and trigger increases in $[Ca^{2+}]_{cyt}$ in incompatible pollen tubes (Franklin-Tong et al., 1993). The rapid elevation in $[Ca^{2+}]_{cyt}$ in the subapical and shank regions to ~1.5 μM in incompatible pollen tubes is accompanied by the disappearance of the apical Ca^{2+} gradient (Franklin-Tong et al., 1997). During the SI response, actin filaments undergo dramatic reorganization; the distinctive longitudinal F-actin bundles disappear and this is accompanied by a large reduction in actin polymer level (Snowman et al., 2002). Afterwards, fine fragments of actin reorganize into larger aggregates and form highly stable actin foci that increase in size over time in SI pollen tubes and persist for at least 3 h (Geitmann et al., 2000; Poulter et al., 2011; Poulter et al., 2010). There is good evidence that elevations in $[Ca^{2+}]_{cyt}$ are upstream of SI-induced actin cytoskeletal rearrangements (Rudd and Franklin-Tong, 2003; Staiger and Franklin-Tong, 2003). Treatment of pollen tubes with the Ca^{2+} ionophore A23187 mimics the SI response, inducing dramatic depolymerization and actin rearrangement into actin foci in pollen tubes (Geitmann et al., 2000; Snowman et al., 2002). The level in actin depolymerization was measured and shown to be far in excess of that required to arrest pollen tube growth (Snowman et al., 2002). Subsequent studies showed that both actin depolymerization and actin stabilization is sufficient to trigger PCD (Thomas et al., 2006). However, to date, the exact mechanisms involved in mediating the dramatic actin alterations and the molecular players involved in this response are largely unknown.

Actin binding proteins (ABPs) are direct regulators of actin dynamics (Pollard, 2016) and transduce cellular stimuli into alterations of the actin architecture, mediating actin cytoskeleton rearrangements in response to various stimuli (Li et al., 2015). Some of them are directly regulated by Ca^{2+} and several ABPs have been shown to bind directly to and be regulated by second messengers (Drøbak et al., 1994; Gungabissoon

et al., 1998; Janmey et al., 1987) or by phosphorylation and dephosphorylation events (Khurana et al., 1997; Zhai et al., 2001). Relevant to the *Papaver* system, a previous study found that that profilin, a G-actin sequestering ABP that is abundant in pollen tubes, does not appear to have sufficient Ca^{2+}-stimulated sequestering activity to account for the level of depolymerization measured during SI (Snowman et al., 2002). Moreover, two further ABPs: cyclase associated protein (CAP) and actin depolymerizing factor (ADF) have been implicated in the regulation of the formation of actin foci in SI pollen tubes, as they colocalize to the actin foci (Poulter et al., 2011; Poulter et al., 2010). Interestingly, fimbrin, a side-binding ABP (McCurdy et al., 2001) did not colocalize to actin foci (Poulter et al., 2011). Villin, a Ca^{2+}-responsive ABP (Kumar et al., 2004; Markus et al., 1997), is a relevant player that mediates actin alterations in pollen tubes in response to the elevation in $[Ca^{2+}]_{cyt}$, but has not previously been studied in relation to the SI response in *Papaver*. Villin homologues were originally identified by biochemical means in plants (Yokota and Shimmen, 1999; Yokota et al., 2003). The function and mechanism of action of villins have been documented extensively in *Arabidopsis* (Huang et al., 2015). Apart from *Arabidopsis* VLN1, which is a simple actin bundler (Huang et al., 2005), other *Arabidopsis* villins have the full suite of villin-related actin regulatory activities, including nucleating actin assembly, capping, severing and bundling actin filaments (Bao et al., 2012; Khurana et al., 2010; Zhang et al., 2010; Zhang et al., 2011). Micromolar-range free Ca^{2+} is sufficient to trigger actin severing activity of *Arabidopsis* villins (Bao et al., 2012; Khurana et al., 2010; Zhang et al., 2010; Zhang et al., 2011), implying that the actin severing activity of villin is biologically relevant within the apical region of pollen tubes where free $[Ca^{2+}]_{cyt}$ reaches about 1 μM to 10 μM (Messerli and Robinson, 1997; Pierson et al., 1994). Indeed, loss of function of *VLN2* and *VLN5* causes accumulation of actin filaments at pollen tube tips (Qu et al., 2013). However, to date, whether or how exactly villins contribute to the dramatic actin alterations induced by SI in pollen tubes lacks direct genetic and cytological evidence.

The demonstration that the *Papaver* SI *S*-determinants have been functionally transferred to *Arabidopsis* (de Graaf et al., 2012; Lin et al., 2015) suggests that the downstream signals and targets involved in modulating the SI response (e.g. alterations to the actin cytoskeleton and triggering of PCD), might be common and conserved among higher plants. Use of *Arabidopsis* as an experimental system enables the use of the powerful *Arabidopsis* genetic approaches and resources to uncover the signaling networks, cellular targets and genes/proteins involved in the SI response in incompatible pollen tubes. It also allows the use of advanced live-cell imaging technologies in conjunction with fluorescent actin markers. Indeed, recent studies suggest that the *Arabidopsis* pollen tube is a great cellular system to perform live cell imaging of actin dynamics (Qu et al., 2017). As many of the molecular players and mechanisms underlying the dramatic rearrangement of the actin cytoskeleton into the punctate actin foci in response to SI remain to be explored, we have made the first step by treating *Arabidopsis thaliana* pollen tubes with the Ca^{2+} ionophore A23187. This drug has previously been shown to increase $[Ca^{2+}]_{cyt}$ in pollen tubes (Diao et al., 2018; Franklin-Tong et al., 1996) and also mimic the SI response in *Papaver* pollen tubes, stimulating the formation of distinctive actin alterations (Snowman et al., 2002) as well as triggering several other SI-related events (Wilkins et al., 2011).

Here we perform live-cell imaging of actin filament dynamics in response to A23187 in *Arabidopsis* pollen tubes, and reveal that actin alteration during this process involves the rearrangement, fragmentation and depolymerization of actin filaments. We found that actin foci form at a very early stage and that they gradually enlarge with the incorporation of fragmented actin structures. We further identify that villin is involved in A23187-triggered actin depolymerization and formation of actin foci in pollen tubes, which requires its Ca^{2+}-responsive actin severing activity. Our findings suggest that fragmentation of actin filaments is a key event during the formation of actin foci and it

is required for efficient actin depolymerization in pollen tubes. Strikingly, we found that villin is also involved in the enlargement of the distinctive punctate actin foci; this stage of remodeling requires villin's actin bundling activity. Our study thus reveals novel molecular details and insights into mechanisms underlying actin alterations in response to A23187 in pollen tubes and provide evidence that villin is a major player in modulating this remodeling.

RESULTS

A23187 triggers alterations of the actin cytoskeleton in *A. thaliana* pollen tubes similar to those observed in the SI response in *Papaver*

To initiate a detailed analysis of the molecular mechanisms potentially involved in mediating similar actin alterations to those triggered by the SI response, we used the ionophore A23187 as a tool to investigate actin reorganization in pollen tubes of *Arabidopsis thaliana*. We treated *A. thaliana* pollen tubes with the Ca^{2+} ionophore A23187 and they were fixed at different time points after treatment and then stained with Alexa-488-phalloidin to visualize F-actin. Untreated control pollen tubes had actin filaments arrayed in prominent actin cables oriented longitudinally in the shank region and a bright apical actin structure (Fig. 1A). After treatment with 10 μM A23187 for 2 min, 10 min and 60 min, respectively, dramatic rearrangements of actin filaments were observed in pollen tubes (Fig. 1A). Actin filaments became fragmented and the amount of thick actin bundles was reduced and actin foci started to form in the pollen tubes after being treated with 10 μM A23187 for 2 min (Fig. 1A). The number of actin foci increased and the size of actin foci enlarged in pollen tubes after treatment with A23187 for 10 min and 60 min compared to those treated with A23187 for 2 min (Fig. 1A).

The observed actin rearrangements in *Arabidopsis* pollen tubes after the treatment with A23187 were very similar to those triggered in *Papaver* pollen tubes during the SI response (Geitmann et al., 2000; Poulter et al., 2010; Snowman et al., 2002) and to those observed in *A. thaliana* pollen tubes expressing the *PrpS* gene (line *At-PrpS*$_1$) when challenged with recombinant PrsS proteins, reconstituting SI in this species (Fig

1B). With SI, actin filaments became fragmented and the amount of thick actin bundles was reduced after 2 min (Fig. 1B). The actin remodeling in response to SI was slower compared to A23187, but foci were forming at 60 min and the size of actin foci was increased at 3 h (Fig. 1B). These data clearly show the striking similarity between the dramatic actin remodeling stimulated by A23187 and SI.

A23187 triggers fragmentation of actin filaments and recruitment of actin fragments to form actin foci in pollen tubes

To trace the dynamic behavior of actin filaments during this process, we monitored *Arabidopsis* pollen tubes expressing *Lat52:Lifeact-eGFP* (Qu et al., 2013) in real-time after treatment with 10 μM A23187. This revealed that, very soon after A23187 treatment, actin filaments undergo rearrangements, exhibited as a conversion of longitudinally arranged actin cables into network-like structures in the pollen tube (Fig. 2A; Fig. S1A). Although the starting time points of actin rearrangement vary between individual pollen tubes, actin rearrangement occurred within 1 min after A23187 treatment. Subsequently, actin filaments became fragmented and these fragmented actin filaments appeared to depolymerize (Fig. 2A, B, Supplemental Movie 1; Fig. S1A, B). The depolymerization of actin filaments was revealed by determining the percentage of "occupancy" of actin filaments, which was evaluated by the parameter of density of actin filaments as described previously (Higaki et al., 2010). As shown in Fig. 2C and Fig. S1C, the percentage of "occupancy" of actin filaments decreased during the treatment of A23187, suggesting that actin filaments underwent depolymerization.

These observations are very similar to previous observations of actin alterations and measurements of depolymerization during the SI response in *Papaver* pollen tubes (Snowman et al., 2002). Accompanied by the fragmentation and depolymerization of actin filaments, actin foci began to form. Soon after actin foci formed, they enlarged during the treatment with A23187 (Fig. 2D), quantified by an increase in fluorescence

intensity (Fig. 2E and Fig. S1D). Again, this is consistent with previous observations and measurements of formation of actin foci during SI in *Papaver* pollen tubes (Poulter et al., 2010), except the timing of actin remodeling is (unsurprisingly) faster with A23187.

In terms of the formation of actin foci in response to A23187 treatment of pollen tubes, we observed several distinct patterns of actin reorganization. One of the patterns starts with the fragmentation of large actin bundles. After the large actin bundles were fragmented into a couple of pieces, these fragmented actin structures were used as templates to recruit small actin structures to promote the formation of the punctate actin foci structures (Fig. 2F, G). Another pattern of actin foci formation started with the greater fragmentation of actin bundles into tiny structures first, and these structures subsequently came together in a manner resembling some sort of aggregation or fusion, to form the large actin foci (Fig. 2H, I). These detailed observations suggest that the formation and enlargement of these actin foci mainly result from the cross-linking of fragmented actin structures. The common feature of these patterns of actin remodeling is that actin filaments or bundles need to be fragmented first, prior to the formation of actin foci. This suggests that A23187 triggers fragmentation or severing of actin structures, which appears to be a prerequisite for the formation of these punctate actin foci. Thus, our study reveals novel, key information about the underlying actin alterations involved in the formation of these distinctive punctate actin foci in pollen tubes in response to A23187.

VLN2, VLN3 and VLN5 Associate with Different Actin Structures in Pollen Tubes after Treated with A23187

To ask which ABP(s) might participate in this A23187-triggered actin alteration process in pollen tubes, the Ca^{2+}-sensitive gelsolin/villin family proteins were considered good candidates, as A23187 is known to trigger increases in $[Ca^{2+}]_{cyt}$. In this regard, VLN2, VLN3 and VLN5 could potentially be involved in this actin alteration process, as they are expressed in pollen (https://www.genevestigator.com/gv/index.jsp; (Honys and

Twell, 2003; Pina et al., 2005)) and shown to be versatile Ca^{2+}-responsive actin regulatory proteins including fragmenting actin filaments (Bao et al., 2012; Khurana et al., 2010; Zhang et al., 2010). We determined the localization of VLN2, VLN3 and VLN5 before and after the addition of A23187 in pollen tubes. We found that VLN2-GFP, VLN3-GFP and VLN5-GFP associated with filamentous structures resembling actin to different extents in normally growing *A. thaliana* pollen tubes in the absence of A23187 (Fig. 3A; (Qu et al., 2013)). After the treatment of pollen tubes with A23187, within a few minutes the VLN2-GFP, VLN3-GFP and VLN5-GFP formed dot-like structures (Fig. 3A; Supplemental Movies 2-4). The formation of these structures started in the apical region and propagated backwards to the shank in pollen tubes and the number of dots increased over time (Fig. 3A). By monitoring the dot-like structures formed by VLN-GFP fusion proteins in real time, we established that their size increased over time (Fig. 3B; Fig. S2). The changes in the pattern of VLN-GFP fusion proteins resembled that of actin after treatment with A23187. In support of this notion, examination of fixed A23187-treated pollen tubes at a later time point revealed that the structures decorated with VLN-GFP fusion proteins in these pollen tubes colocalized with Alexa-568-phalloidin stained punctate actin foci. This demonstrates that the VLN-GFPs colocalize with F-actin (Fig. 3C). Taken together, these data implicate the involvement of villins in these actin remodeling processes in pollen tubes.

VLNs are Required for the Fragmentation and Depolymerization of Actin Filaments in Response to A23187 in Pollen Tubes

To determine whether and to what extent villins contribute to actin alterations in response to A23187 in *A. thaliana* pollen tubes, we visualized the actin cytoskeleton in villin loss-of-function mutant pollen tubes treated with A23187 and compared it to that in WT pollen tubes. We found that actin alterations in villin loss-of-function mutant pollen tubes were perturbed when compared to that in WT pollen tubes (Fig. 4A). In particular, the loss of function of *VLN5* had a more profound effect on A23187 treatment-induced changes in the actin cytoskeleton in pollen tubes when compared to

that in WT or *vln2* single mutant pollen tubes (Fig. 4A). Specifically, at 60 min after A23187 treatment, we found that there were more fragmented actin bundles in *vln5* pollen tubes, whereas most actin filaments were converted into actin foci in WT, *vln2* or *vln5* single mutant pollen tubes (Fig. 4A). This suggests that loss of function of *VLN5* impairs the fragmentation of actin filaments or actin bundles after the treatment with A23187. In addition, we found that the relative amount of fragmented actin bundles versus actin foci is substantially higher in the *vln2 vln5* double mutant pollen tubes when compared to that in *vln5* pollen tubes (Fig. 4A). Strikingly, we found that the formation of actin foci was severely impaired in *vln2 vln3 vln5* triple mutant pollen tubes (Fig. 4A), suggesting that these villins are redundantly required for these actin alterations in pollen tubes in response to A23187.

To quantitatively determine the amount of actin filaments in pollen tubes derived from WT and villin loss-of-function mutants, we skeletonized actin filament staining images; representative skeletonized images after treated with A23187 for 60 min are shown in Fig. 4B. We found that the density of actin filaments was significantly higher in the villin loss-of-function mutant pollen tubes compared to that in WT pollen tubes, with the exception of *vln2* (Fig. 4B, C). These data, showing that loss of function of villins impairs both actin depolymerization and the formation of punctate actin foci in pollen tubes in response to A23187 suggest that villins are involved in mediating these processes, acting in concert to remodel actin to form these structures. Moreover, this implicates villins are also involved in the highly similar actin remodeling observed during the SI response in *Papaver*.

Severing-deficient VLN5 Has Reduced Activity in Fragmenting Actin Filaments or Bundles in Response to A23187 in Pollen Tubes

Next, we wondered whether the severing activity of villins is involved in actin alterations in response to A23187 in pollen tubes. We decided to abolish the severing

activity of villins using VLN5 as the representative villin. The severing deficient version of VLN5, designated as VLN5^{SD}, was generated as described previously (Fig. 5A; (Revenu et al., 2007)). We initially performed dilution-mediated actin depolymerization experiments to determine the actin depolymerizing activity of recombinant VLN5 and VLN5^{SD} proteins (Fig. 5B; (Zhang et al., 2010)). We found that VLN5 promotes actin depolymerization whereas VLN5^{SD} lacked such activity (Fig. 5C). Strikingly, in contrast, VLN5^{SD} stabilizes actin filaments from dilution-mediated actin depolymerization (Fig. 5C). In addition, through direct visualization of individual actin filaments by total internal reflection fluorescence microscopy (TIRFM), we found that while VLN5 efficiently severed actin filaments, VLN5^{SD} lacked such actin severing activity (Fig. 5D, E). These data demonstrate that VLN5^{SD} fails to depolymerize and sever actin filaments. However, we found that VLN5^{SD} retained a similar actin bundling activity compared to VLN5 at 0.4 μM (Fig. 5F, G). Interestingly, VLN5^{SD} had a slightly higher ($P = 0.03$) actin bundling activity than VLN5 at a lower concentration (0.2 μM; Fig. 5G). Nonetheless, these data together demonstrate that VLN5^{SD} retains virtually normal actin bundling activity but is defective in severing actin filaments.

We next transformed *VLN5* and *VLN5*^{SD} into the *vln2 vln5* double mutant under the control of *VLN5*'s native promoter (Fig. S3A) to determine how the actin severing activity of VLN5 might be involved in regulating actin alterations in response to A23187 in pollen tubes. We found that the introduction of VLN5 can rescue, whereas the introduction of VLN5^{SD} cannot rescue, the defective fragmentation of actin filaments or bundles and the formation of actin foci in *vln2 vln5* mutant pollen tubes (Fig. 5H). In addition, we found that the introduction of VLN5^{SD} cannot rescue the defects in actin depolymerization in response to A23187 treatment in *vln2 vln5* mutant pollen tubes by determining the percentage of occupancy of actin filaments (Fig. 5I, J). This suggests that the severing activity of VLN5 (which is known to be Ca^{2+}-dependent (Zhang et al., 2010)) contributes to its role in driving A23187-triggered actin depolymerization. Our data shows that VLN5^{SD} cannot fully rescue the defects in A23187-triggered actin alterations compared to VLN5 in pollen tubes, particularly in terms of actin filament fragmentation and the formation of actin foci (Fig. 5K). This suggests that the actin severing activity of VLN5 is required for the fragmentation and depolymerization of actin filaments in response to A23187 in pollen tubes.

The Bundling Activity of VLN5 is involved in the Enlargement of Actin Foci

To determine whether the bundling activity of villins might be involved in driving actin alterations responsible for the formation of the large punctate actin foci in pollen tubes in response to A23187, we used VLN5 as the representative villin to address this question. We decided to remove the bundling activity of VLN5 by deleting its linker and headpiece domain as previously done for VLN3 (van der Honing et al., 2012). The truncated version of VLN5 with the deletion of linker and headpiece domain was designated as VLN5ΔHL (Fig. 6A, B). We found that both VLN5ΔHL and VLN5 can bind to F-actin using high-speed F-actin cosedimentation experiments (Fig. S4A-D). However, using low-speed F-actin cosedimentation experiments, we found that the actin bundling activity of VLN5ΔHL was significantly reduced compared to VLN5 (Fig. 6C, D), especially at higher concentrations, when the VLN5ΔHL mutant had only 12%

bundling activity (P = 0.000004) compared to VLN5 (Fig. 6D). The decrease in the bundling activity of VLN5ΔHL was also confirmed by direct visualization of filamentous actin structures with fluorescence light microscopy (Fig. 6E). However, using direct visualization of actin filaments with TIRFM, we found that VLN5ΔHL severed actin filaments just as efficiently as VLN5 (Fig. 6F, G). This demonstrates that its severing activity was not affected.

We next transformed *VLN5ΔHL* into the *vln2 vln5* mutant under the control of *VLN5* native promoter (Fig. S3B), and found that actin filaments or bundles could be fragmented and converted into actin foci (Fig. 6H). Interestingly, we found that the size of actin foci was smaller in VLN5p:VLN5ΔHL (*vln2 vln5*) pollen tubes when compared to that in VLN5p:VLN5 (*vln2 vln5*) pollen tubes under the same conditions (Fig. 6H, I). Visualization of the actin cytoskeleton in pollen tubes at different time points after treatment with A23187 showed the increase in the fragmentation of actin structures in pollen tubes within 2 min and subsequent accumulation of punctate actin foci (Fig. 6J), further demonstrating that VLN5ΔHL can fragment actin structures *in vivo*. Quantification of the "occupancy" of actin structures showed that VLN5ΔHL was able to depolymerize actin filaments in response to A23187 treatment of pollen tubes (Fig. 6K). However, we do not currently know why VLN5ΔHL cannot depolymerize actin filaments as efficiently as VLN5 in pollen tubes after A23187 treatment (Fig. 6K). Pollen tubes with the VLN5ΔHL retained the capability to promote the formation of actin foci, but failed to enlarge actin foci in response to A23187 in pollen tubes. This was confirmed by direct visualization of actin filaments decorated with Lifeact-mCherry after treated with A23187 in pollen tubes (Fig. 6L, M). These findings were also supported by data showing that VLN5ΔHL colocalizes with actin foci in A23187-treated pollen tubes (Fig. S4E), but the enlargement of VLN5ΔHL-decorated structures was impaired severely (Fig. S4F). These observations demonstrate that the initial stages of actin foci formation in the VLN5p:VLN5ΔHL (*vln2 vln5*) pollen tubes compared to

either WT or VLN5p:VLN5 (*vln2 vln5*) pollen tubes are normal, while the enlargement of actin foci is impaired (Fig. 6N). Because VLN5ΔHL has dramatically reduced bundling activity due to removal of the linker and headpiece domains, these data implicate that the bundling activity of VLN5 is required for the enlargement of actin foci in response to the elevation in $[Ca^{2+}]_{cyt}$ in pollen tubes. Thus, together our data suggest that the formation of the actin foci involves at least two steps, both involving villin: (1) the severing of actin filament bundles, which will allow rapid/efficient depolymerization and (2) bundling of actin filament fragments to form large actin foci.

DISCUSSION

The actin cytoskeleton is a major target of the signaling networks in eukaryotic cells (Li et al., 2015). How the actin cytoskeleton responds to upstream signaling events and achieves reorganization to meet cellular demands is a fascinating topic with many unanswered questions. ABPs are direct regulators of actin dynamics that transduce cellular stimuli into alterations of the actin architecture (Hussey et al., 2006; Smith and Oppenheimer, 2005; Staiger and Franklin-Tong, 2003). The SI response in *Papaver rhoeas* pollen tubes has a relatively well characterized Ca^{2+}-mediated signal transduction network that induces dramatic alterations to the actin cytoskeleton in incompatible pollen tubes involving the formation of distinctive punctate actin foci (Geitmann et al., 2000; Poulter et al., 2010; Snowman et al., 2002) necessary and sufficient to trigger PCD in this system (Thomas et al., 2006; Wang et al., 2019; Wilkins et al., 2014). These actin foci are rather unusual as they are highly stable; once formed, they are resistant to disassembly by 1 μM Latrunculin B (LatB) under conditions that remove virtually all detectable F-actin in normally growing pollen tubes (Snowman et al., 2002; Thomas et al., 2006). This sets them apart from many other actin-based structures reported. Currently, there are no explanations for the formation or unusual dynamic properties of these structures. The molecular players and mechanisms underlying the actin alterations in pollen tubes in response to SI signaling remains

largely unexplored, except for a study showing that ADF and CAP co-localize with these actin foci during their formation; somewhat surprisingly, fimbrin, which cross-links and stabilizes actin filaments in plant cells (Kovar et al., 2000b) did not colocalize with the SI-induced actin foci (Poulter et al., 2010).

Here we performed live-cell imaging of actin dynamics to investigate the formation of actin foci in *Arabidopsis* pollen tubes, using the calcium ionophore A23187 as a trigger. This drug, which has been shown to raise $[Ca^{2+}]_{cyt}$ artificially in pollen tubes (Diao et al., 2018; Franklin-Tong et al., 1996), mimics the SI response in *Papaver* pollen tubes as it induces similar alterations to the actin cytoskeleton in *Papaver* pollen tubes as the SI response (Snowman et al., 2002). Because A23187 has previously been demonstrated to increase $[Ca^{2+}]_{cyt}$ we infer that A23187 triggers increases in $[Ca^{2+}]_{cyt}$ in these *A. thaliana* pollen tubes, even though we have not assessed this here. However, regardless of this, A23187 provides a useful, simple tool to trigger the formation of punctate actin foci in order to study both the nature of their formation and ABPs involved in this process. Use of *Arabidopsis* has enabled us to investigate the role of Ca^{2+}-responsive villins using cytological and genetic approaches not available in *Papaver*. This has enabled us to show for the first time that villins are involved in mediating actin alterations very similar to those observed during the SI response in *Papaver* pollen tubes. Moreover, we provide important insights into the mechanistic details of what is involved in the formation of the distinctive punctate actin foci. Treatment with A23187 triggers the formation of punctate actin foci in *A. thaliana* pollen tubes, which is one of the characteristic features shown in *Papaver* SI pollen tubes (Rudd and Franklin-Tong, 2003; Staiger and Franklin-Tong, 2003), suggesting that *A. thaliana* might have all the components necessary for SI-triggered Ca^{2+}-dependent signaling network in *Papaver* pollen tubes.

Based on our findings, we propose a simple model describing actin alterations in response to the A23187 treatment of the pollen tube incorporating the involvement of the Ca^{2+}-responsive ABP, villin (Fig. 7). Specifically, we have imaged at least four

distinct configurations of actin: (i) normal actin configuration of longitudinal bundles in normally growing pollen tubes (Fig. 7A), (ii) fragmentation of longitudinal actin bundles involving the severing activity of villin, which will allow more effective depolymerization that drives the breakdown of filaments (Fig. 7B). Next the formation of actin foci from actin fragments involves (iii) a bundling activity, which involves villin (Fig. 7C) and (iv) enlargement of the foci, which also involves villin (Fig. 7D). Because the deletion of the linker and headpiece domains prevents the enlargement of actin foci, this provides evidence that this later stage is achieved by the crosslinking of fragmented actin structures.

As A23187 has been shown to increase $[Ca^{2+}]_{cyt}$ (Diao et al., 2018; Franklin-Tong et al., 1996) these data together suggest that an elevation in $[Ca^{2+}]_{cyt}$ stimulates the initial fragmentation and depolymerization of actin filaments in pollen tubes. This could cause disruption of the normal actin configuration and a reduction in the amount of actin filaments observed here. Our data are consistent with previous findings from *Papaver* showing a severe reduction in the amount of actin filaments in pollen tubes after SI-induction (Geitmann et al., 2000; Snowman et al., 2002; Thomas et al., 2006). An attempt was previously made to assess the potential contribution of profilin to the actin depolymerization in response to the elevation in $[Ca^{2+}]$ *in vitro*, as actin monomer sequestering activity of profilin is stimulated by Ca^{2+} (Kovar et al., 2000a) and the concentration of profilin is almost equal molar to actin in pollen (Gibbon et al., 1999; Snowman et al., 2002; Vidali and Hepler, 1997). However, this study showed that the elevation in $[Ca^{2+}]$ could only account for a 10-16% reduction in the amount of actin filaments (Snowman et al., 2002), implicating that other ABPs contribute to this actin depolymerization process, as the SI response can cause 60-70% depolymerization of actin in pollen (Snowman et al., 2002; Thomas et al., 2006).

Based on the observations that actin filament fragmentation events observed are very frequent after A23187 treatment, the actin severing proteins ADF/cofilin or villin/gelsolin are likely contributors. As SI in *Papaver* triggers both increases in

$[Ca^{2+}]_{cyt}$ (Franklin-Tong et al., 1997; Franklin-Tong et al., 1993; Wu et al., 2011) and acidification of cytoplasm (Wilkins et al., 2015) in SI-induced pollen tubes, ADF is an unlikely candidate for this actin fragmentation process as the severing activity of plant ADFs is reduced by Ca^{2+}-dependent protein kinases (Allwood et al., 2001; Dong and Hong, 2013) and they prefer alkaline conditions for severing (Maciver and Hussey, 2002). We considered the calcium-responsive villins/gelsolins as likely candidates for this depolymerization/fragmentation process as a previous study demonstrated that a gelsolin purified from *Papaver* pollen fragments actin filaments and acts in concert with profilin to promote substantial actin depolymerization (Huang et al., 2004). Thus, we wondered whether *Arabidopsis* villins might perform similar functions by fragmenting actin filaments and capping the barbed end of actin filaments to promote actin depolymerization via acting in concert with profilin in response to elevations in $[Ca^{2+}]_{cyt}$ in pollen tubes. Since the *Arabidopsis* genome only encodes villin-like genes (Klahre et al., 2000), the pollen-expressed villins are likely candidates involved in this actin alteration process. Here we have established a clear role for villin in the early actin remodeling events involving severing activity in response to A23187. As the severing activity of villins is Ca^{2+}-responsive (Bao et al., 2012; Khurana et al., 2010; Kumar et al., 2004; Markus et al., 1997; Wu et al., 2015; Yokota et al., 2005; Zhang et al., 2010; Zhang et al., 2011) and A23187 is known to increase $[Ca^{2+}]_{cyt}$ (Diao et al., 2018; Franklin-Tong et al., 1996), this suggests that severing is an important early event triggered by increases in $[Ca^{2+}]_{cyt}$, responsible for breaking down long actin filament bundles to generate more filament ends for monomer dissociation. We propose that villin activity is likely to act in concert/cooperatively with the Ca^{2+}-responsive monomer sequestering activity of profilin (Kovar et al., 2000a).

Later another activity is evident, as the fragmented actin filaments or actin bundles were observed to be brought together to form the punctate actin foci. We provide evidence that villins mediate the formation and enlargement of the actin foci in pollen tubes. Our

observations suggest that this mainly results from the cross-linking of fragmented actin structures; this is further supported by our findings that villins associate with the actin foci during their formation and the actin bundling activity of villins is required for the enlargement of actin foci. Thus, our data also implicates a role for villins in a bundling activity involved in the formation of punctate foci in pollen tubes. It was previously shown that the SI-induced actin foci are highly stable, being resistant to 1 μM LatB (Poulter et al., 2010). Our findings that the actin foci are decorated by villins helps explain why the actin foci are very stable, as it has been shown that villin 1-decorated actin filaments are resistant to the action of ADF and LatB (Huang et al., 2005).

However, exactly how and why these structures form as well as what their function is still largely unknown. It is worth mentioning that a previous study revealed ADF co-localizing with the actin foci (Poulter et al., 2010), which makes sense if there is a change in activity from severing to bundling due to pH. Therefore, it is possible that ADF and villins may act in concert/cooperatively. Moreover, CAP may also be involved in this remodeling together with villins, as CAP was previously colocalized with these actin foci (Poulter et al., 2010). In budding yeast (*Saccharomyces cerevisiae*) the formation of F-actin "bodies" is dependent on Srv2p/CAP activity (Gourlay et al., 2004); moreover, this study showed that a decrease in actin dynamics can induce cell death involving reactive oxygen species (ROS). As it has been shown that both actin depolymerization and stabilization can stimulate PCD in pollen tubes (Thomas et al., 2006), this further suggests that mechanistically, the stabilization of the actin cytoskeleton somehow plays a role in modulating PCD in these pollen tubes. Indeed, it has been shown that SI stimulates increases in ROS and that A23187 also does so; downstream, actin foci are formed and PCD involving a DEVDase activity is triggered (Wilkins et al., 2011). However, exactly what physiological functions these foci perform and how they achieve these outcomes is not known. Nonetheless, our study yields significant insights into the mechanisms involved in the formation and enlargement of actin foci in pollen tubes.

In summary, our study uncovers molecular details and mechanism underlying actin alterations in response to A23187 and assumed accompanying elevation in $[Ca^{2+}]_{cyt}$ in pollen tubes. Because the events observed here are so similar to those observed during an authentic SI response, this study provides significant insights into the cellular mechanisms of the SI response in *Papaver* pollen tubes. Nevertheless, it will be important in the future to study the SI response in *Arabidopsis* lines expressing PrpS to investigate and confirm that these events are involved in authentic SI responses and to uncover further details of the mechanisms and ABPs involved in this actin remodeling.

Methods

Plant Materials and Growth Condition

Arabidopsis Columbia ecotype (Col-0) was used as the wild type plant. The information of T-DNA insertion mutants of *VLN2*, *VLN3* and *VLN5* as well as the transgenic plants harboring GFP fusion constructs: *pK7FWG2-VLN5p*:*VLN5-EGFP;vln2*, *pCambia1301-VLN3p:VLN3-EGFP;vln3* and *pK7FWG2-VLN5p:VLN5-EGFP;vln5* had been described previously (Bao et al., 2012; Zhang et al., 2010). *Arabidopsis* transgenic plants harboring VLN5 that was deficient in either severing or bundling actin filaments were generated as described below. The *At-ntp303p::PrpS$_1$-GFP* transgenic lines are described in (de Graaf et al., 2012). Briefly, *Col-0 A. thaliana* was transformed with the Ti vector pGreen0029-*ntp303p::PrpS$_1$-GFP*. The ntp303 is a pollen-specific promoter. This line is referred in the text as *At-PrpS$_1$* for simplicity. *Arabidopsis* plants were grown on half-strength Murashige and Skoog media or in soil at 22 °C under a photoperiod regime of 16 h light and 8 h dark.

Plasmid Construction

To generate the recombinant $VLN5^{SD}$ protein (severing deficient VLN5; Fig. 5A), we made a prokaryotic expression construct to produce, the necessary 934bp fragment, as described previously (Revenu et al., 2007). Briefly, this was amplified using pET23d-VLN5 (Zhang et al., 2010) as the temperate with primer pair $VLN5CDS_F$/$VLN5CDS_R$ (Table S1). The amplified fragment was subsequently moved into pMD19-T that was

used as the template for the subsequent PCR amplification using primer pairs $VLN5^{SD}{}_{1F}$/$VLN5^{SD}{}_{1R}$ and $VLN5^{SD}{}_{2F}$/$VLN5^{SD}{}_{2R}$ (Table S1). The fragment digested with *Kpn*I/*Mlu*I was moved into pET23d-VLN5 restricted with the same enzymes to generate the pET23d-$VLN5^{SD}$. To construct the pET23d-VLN5ΔHL plasmid, the PCR product was amplified with primer pair $VLN5\Delta HL_F$/$VLN5\Delta HL_R$ (Table S1) using pET23d-VLN5 (Zhang et al., 2010) as the template and the error-free PCR fragment restricted with *Sac*I/*Eco*RI was subsequently moved into pET23d to generate pET23d-VLN5ΔHL.

Protein Purification

To generate VLN5, $VLN5^{SD}$ and $VLN5^{\Delta HL}$ recombinant proteins, the plasmids pET23d-VLN5, pET23d-$VLN5^{SD}$ and pET23d-$VLN5^{\Delta HL}$ were transformed into the *Escherichia coli* BL21 DE3 strain. After induction with the addition of Isopropyl ß-D-1-thiogalactopyranoside (final concentration, 0.4 mM) at 16 °C for 12~16 h, the cells were collected by centrifugation. They were subsequently lysed by sonication, and the protein in the supernatant was precipitated with $(NH_4)_2SO_4$ (final concentration = 45%). After centrifugation (10,000 g, 30 min, 4°C), the pellet was re-suspended in Binding Buffer (5 mM imidazole, 250 mM KCl, 25 mM Tris-HCl, pH 8.0). After clarification at 100,000 *g* for 30 min at 4°C, the supernatant was loaded onto a Nickel sepharose column, and purification was performed according to manufacturer's instruction. The purified protein was dialyzed against 5 mM Tris-HCl, pH 8.0. The protein was aliquoted and freshly frozen in liquid nitrogen and stored at -80 °C. Skeletal muscle actin was purified according to previously published methods (Pollard, 1984; Spudich and Watt, 1971). To monitor the kinetic actin assembly and disassembly, actin was conjugated with pyrene iodoacetamide as described previously (Pollard, 1984). To directly visualize the dynamics of individual actin filaments, actin was labeled with Oregon-green as described previously (Amann and Pollard, 2001).

RT-PCR

Pollen was collected from freshly opened *Arabidopsis thaliana* flowers as described previously (Chang and Huang, 2015; Chang and Huang, 2017). Total pollen RNA was extracted by Eastep® Super Total RNA Extraction Kit (Promega) following manufacturer's instructions. 5 μg RNA was used for reverse transcription by MMLV reverse transcriptase (Promega) to synthesize cDNA. To determine the transcript levels of *VLN5*^{SD} and *VLN5ΔHL*, transcripts of *VLN5*^{SD} and *VLN5ΔHL* were amplified with primer pair q*VLN5* F/q*VLN5* R (Table S1). *eIF4A* was amplified with primer pair *eIF4A* F/*eIF4A* R (Table S1) as the internal control. Amplification was completed using GenStar qPCR Green Mix (Genstar), running on an Applied Biosystems® 7500 fast Real-Time PCR System. The transcription levels of genes were calculated using the $2^{-\Delta Ct}$ method (Livak and Schmittgen, 2001), in which $\Delta Ct = Ct_{(eIF4A)} - Ct_{(gene)}$.

***A. thaliana* Pollen Germination, growth and treatment with A23187**

In vitro germination of *A. thaliana* pollen from wildtype and villin loss-of-function mutants was performed as described previously (Ye et al., 2009). For live-cell imaging, *A. thaliana* lines expressing *Lat52:Lifeact-eGFP* were used. Briefly, the newly open flowers were collected and dipped on the surface of pollen germination medium (GM: 1 mM $CaCl_2$, 1 mM $Ca(NO_3)_2$, 1 mM $MgSO_4$, 0.01% (w/v) H_3BO_3, 18% (w/v) sucrose; solidified with addition of 0.8% (w/v) agarose) and incubated at 28 °C under high humidity for ~3 h to allow growth of pollen tubes. After the average length of pollen tubes reached ~150 μm, A23187 (10 or 50 μM in liquid GM) was added onto the surface of the solid GM containing pollen tubes. After incubation for various periods of time at 28 °C, pollen tubes were fixed and subjected to staining with Alexa-488 phalloidin as described below. Alternatively, to visualize the dynamics of actin filaments in pollen tubes after treatment with A23187, pollen tubes expressing *Lat52:Lifeact-eGFP* were observed immediately after the application of A23187 with a spinning disk confocal microscope, as described below.

A. thaliana At-PrpS$_1$* pollen treatment for the SI bioassay *in vitro

Full details of the the *At-PrpS$_1$-GFP* line and reconstituting the SI response in an *in vitro* bioassay using this line are described in (de Graaf et al., 2012). Briefly, we grew the pollen from this line *in vitro* to obtain an average length of about 150 μm, before adding recombinant PrsS$_1$ (Foote et al., 1994) at 20 ng.μl^{-1} to give a cognate PrpS$_1$-PrsS$_1$ interaction to trigger a SI response. After incubation for various periods of time at 25 °C, pollen tubes were fixed and subjected to staining with Alexa-488 phalloidin as described below.

Visualization of Actin Filaments in Fixed *Arabidopsis* Pollen Tubes

For the A23187 experiments, actin filaments in *A. thaliana* pollen tubes were revealed by staining with Alexa-488 phalloidin as described previously (Wu et al., 2010). Briefly, when the average length of pollen tubes reached ~150 μm, 300 μM N-(maleimidobenzoyloxy)-succinimide (MBS) in liquid GM was added and incubated for 1 h at 28 °C. The samples were subsequently washed with TBS-T (200 mM NaCl, 400 mM sucrose and 0.05% Nonidet P-40 in 50 mM Tris-HCl, pH 7.5) three times. After washing, 200 nM Alexa-488 phalloidin (Invitrogen) was added to the sample and incubated at 4 °C, overnight. The samples of phalloidin-stained pollen tubes were observed under an Olympus FluoView FV1000 confocal microscope equipped with a ×100 UAPON objective (numerical aperture of 1.49). The z-series images were collected with the size of z-step set at 0.7 μm.

For the SI experiments, actin filaments in *A. thaliana* pollen tubes were revealed by staining with Alexa-488 phalloidin according to (Wilkins et al., 2011). Briefly, the SI response was stopped by adding MBS in liquid GM to a final concentration of 400 μM and incubated for six minutes at room temperature. The samples were fixed with 2 % formaldehyde for 30 min, followed by washes in TBS (50 mM Tris-HCl, pH 7.4, 200 mM NaCl). Pollen tubes were permeabilised by treatment in TBS + 0.1% of Triton X-100 for 40 min. F-actin was labeled by adding 66 nM rhodamine phalloidin for >30

min at room temperature. Phalloidin-stained pollen tubes were observed under a Leica SP8 Inverted scanning confocal microscope equipped with a ×100 CS2 objective (numerical aperture of 1.40). The z-series images were collected with the size of z-step set at 0.7 μm.

Visualization of the Dynamics of Actin Filaments in *Arabidopsis* Pollen Tubes

To visualize the dynamics of actin filaments, *Arabidopsis* pollen tubes expressing *Lat52:Lifeact-eGFP* were observed under a Olympus DSU-IX81 spinning disc confocal microscope equipped with a ×100 oil objective (1.4 numerical aperture). The time-lapse z-series images were collected at 2 s intervals with the z step set at 0.5 μm. The excitation wavelength was set at 488 nm, and the emission wavelength was set at 505–545 nm.

Image Analysis

Image processing and measurements were performed using ImageJ software (version 1.51s, http://imagej.nih.gov/ij). To analyze the size of the actin foci in pollen tubes, Z-stack images of actin foci were selected using the "rectangle" tool and the mean grey value of the selected region was calculated by "Analyze-Measure" plugin. To illustrate the actin distribution after A23187 treatment (Fig 4B), Z-stack images were thresholded to create a binary image, followed by a skeletonization procedure (Process-Binary-Skeletonize) so all actin filaments were shown as black, rather than grey-scale. Output images were subsequently made into full projections that were subsequently used for the quantification of the "occupancy" of actin filaments in pollen tubes. The regions of interest (r.o.i.) in pollen tubes were selected using the built in "Polygon selection tool". The total number of pixels and the number of black pixels in the images was counted. Occupancy is defined as the ratio that the number of black pixels divided by the total number of pixels in the r.o.i.. Thus, number of black pixels gave a quantification of actin microfilaments.

To measure the size of actin foci, Z-stack images were thresholded to create a binary image, then the region of interest in pollen tubes were selected by "Polygon selection

tool" in ImageJ. The outlines of foci were analyzed by the "Analyze particles" plugin in ImageJ, and the size of the actin foci was measured by "Measure" plugin in ImageJ. Foci with area smaller than 0.04 μm^2 were dropped from the measurements in order to avoid the background noise. In addition, foci with area larger than 2 μm^2 were also discounted in order to avoid the inclusion of multiple foci that cannot be separated automatically.

High-speed and Low-speed F-actin Cosedimentation Assays

High-speed and low-speed F-actin cosedimentation assays were performed according to previously published methods (Kovar et al., 2000b). Preassembled actin filaments at 3 μM were incubated with various concentrations of VLN5 or its variants in 1×KMEI reaction system (50 mM KCl, 1 mM $MgCl_2$, 1 mM EGTA and 10 mM imidazole, pH 8.0) at room temperature for 30 min, the mixtures were subsequently centrifuged at 13,600 *g* at 4 °C for 30 min for low-speed F-actin cosedimentation experiments. For high-speed F-actin cosedimentation experiments, the mixtures were centrifuged at 160,000 *g* at 4 °C for 1 h. The supernatants and the pellets were resolved by SDS-PAGE and stained with Coomassie Brilliant Blue R. The relative amount of protein in supernatants and pellets was quantified by densitometry.

Dilution-mediated Actin Depolymerization Assay

Dilution-mediated actin depolymerization assay was performed as previously described (Huang et al., 2003; Shi et al., 2013). Briefly, preassembled actin filaments (50% pyrene-labeled) at 5 μM were incubated with VLN5 or its variants for 5 min at room temperature, the mixture was then diluted 50-fold with G buffer (5 mM Tris-HCl, pH 8.0, 0.2 mM ATP, 0.1 mM $CaCl_2$, 0.5 mM DTT, and 0.1 mM imidazole) to induce actin depolymerization. Actin depolymerization was traced by monitoring the changes in pyrene fluorescence with a QuantaMaster Luminescence QM 3 PH Fluorometer (Photon Technology International, Inc.) with the excitation and emission wavelengths set at 365 nm and 407 nm, respectively.

Fluorescence Light Microscopy of Actin Filaments

The experiment was performed according to previously published methods (Zhang et al., 2016; Zhang et al., 2019). Briefly, F-actin at 2 μM was incubated with 500 nM VLN5 or its protein variants in the presence of 2 μM rhodamine-phalloidin (Sigma-Aldrich) in 1× KMEI for 30 min at room temperature. The mixtures were subsequently diluted to 50 nM in TIRF buffer before the observation under a BX53 microscope (Olympus) equipped with a 60×, 1.42–numerical aperture oil objective. The images were acquired with Olympus DP80 camera, using Cell Sens Standard 1.12 software.

Direct Visualization of Actin Filament Severing by TIRFM *in vitro*

This experiment was performed according to previously described methods (Jiang and Huang, 2017; Kuhn and Pollard, 2005). Briefly, 50% rhodamine labeled rabbit muscle actin was preclarified at 200,000*g* for 2 h at 4°C, and then this actin at 10 μM was preassembled at room temperature in the dark. The prepared flow chambers were coated with 10 nM NEM-myosin for 2 min, followed by consecutive washes with HS-BSA buffer (50 mM Tris-HCl, pH 7.5, 600 mM NaCl, 1% BSA) and LS-BSA buffer (50 mM Tris-HCl, pH 7.5, 150 mM NaCl, 1% BSA) for 2 min. They were then washed with TIRF buffer (50 mM KCl, 1 mM $MgCl_2$, 1 mM EGTA, 10 mM imidazole, 100 mM DTT, 0.2 mM ATP, 15 mM glucose, 0.5% methylcellulose, 20 $mg \cdot ml^{-1}$ catalase,

100 mg·ml^{-1} glucose oxidase, pH 7.4). After moving to the microscope stage, preassembled actin filaments at 500 nM in TIRF buffer were injected into the flow cell and incubated for 5 min in the dark. After finding the microscopic field of interest, VLN5 and its protein variants or the control buffer diluted in TIRF buffer containing 1.0 μM free Ca^{2+} was injected into the flow chambers. Actin filaments were observed by Olympus IX-71 microscope equipped with a ×100, 1.45–numerical aperture Planapo objective (Olympus) by TIRF illumination. After finding the focal plane, time-lapse images were captured at 3 s intervals by Hamamatsu ORCA-EM-CCD camera (model C9100-12) driven by Micro-Manager software (www.micro-manager.org; v1.4; MMStudio). The severing activity of VLNs were quantified by measuring the average actin filament severing frequency (at least 15 actin filaments ⩾ 5 μm were chosen from each treatment), which was defined as the number of breaks per unit filament length, per unit time (breaks.μm^{-1}.s^{-1}) (Khurana et al., 2010; Zhang et al., 2010).

Acknowledgements

This work was supported by the grants from National Natural Science Foundation of China (31970180 and 31671390) and the funding from Tsinghua-Peking Center for Life Sciences. Research in the labs of MB and VEF-T is funded by the Biotechnology and Biological Sciences Research Council (grant BB/P005489/1).

Author Contributions

S.H. conceived this project, and S.H., X.Q., and W.Z., designed this research; W.Z., X.Q., Y.Z., and L.W. performed the research; X.Q., W.Z., Y.Z., M.B., V.E.F.-T., L.W., Y.X., and S.H. analyzed the data; W.Z., S.H., and VEF-T wrote the manuscript with the inputs from all authors.

REFERENCES

Allwood, E.G., A.P. Smertenko, and P.J. Hussey. 2001. Phosphorylation of plant actin-depolymerising factor by calmodulin-like domain protein kinase. *FEBS Lett*. 499:97-100.

Amann, K.J., and T.D. Pollard. 2001. Direct real-time observation of actin filament branching mediated by Arp2/3 complex using total internal reflection fluorescence microscopy. *Proc Natl Acad Sci U S A*. 98:15009-15013.

Bao, C., J. Wang, R. Zhang, B. Zhang, H. Zhang, Y. Zhou, and S. Huang. 2012. *Arabidopsis* VILLIN2 and VILLIN3 act redundantly in sclerenchyma development via bundling of actin filaments. *Plant J*. 71:962-975.

Bedinger, P.A., K.J. Hardeman, and C.A. Loukides. 1994. Travelling in style: the cell biology of pollen. *Trends Cell Biol*. 4:132-138.

Cardenas, L., J.E. Thomas-Oates, N. Nava, I.M. Lopez-Lara, P.K. Hepler, and C. Quinto. 2003. The role of nod factor substituents in actin cytoskeleton rearrangements in *Phaseolus vulgaris*. *Mol Plant Microbe Interact*. 16:326-334.

Cardenas, L., L. Vidali, J. Domnguez, H. Prez, F. Snchez, P.K. Hepler, and C. Quinto. 1998. Rearrangement of actin microfilaments in plant root hairs responding to rhizobium etli nodulation signals. *Plant Physiol*. 116:871-877.

Chang, M., and S. Huang. 2015. *Arabidopsis* ACT11 modifies actin turnover to promote pollen germination and maintain the normal rate of tube growth. *Plant J*. 83:515-527.

Chang, M., and S. Huang. 2017. Rapid Isolation of Total Protein from *Arabidopsis* Pollen. *Bio Protoc*. 7:e2227.

de Graaf, B.H., S. Vatovec, J.A. Juarez-Diaz, L. Chai, K. Kooblall, K.A. Wilkins, H. Zou, T. Forbes, F.C. Franklin, and V.E. Franklin-Tong. 2012. The *Papaver* self-incompatibility pollen S-determinant, PrpS, functions in *Arabidopsis thaliana*. *Curr Biol*. 22:154-159.

Diao, M., X. Qu, and S. Huang. 2018. Calcium imaging in *Arabidopsis* pollen cells using G-CaMP5. *J Integr Plant Biol*. 60:897-906.

Dong, C.H., and Y. Hong. 2013. *Arabidopsis* CDPK6 phosphorylates ADF1 at N-terminal serine 6 predominantly. *Plant Cell Rep*. 32:1715-1728.

Drøbak, B.K., P.A.C. Watkins, R. Valenta, S.K. Dove, C.W. Lloyd, and C.J. Staiger. 1994. Inhibition of plant plasma membrane phosphoinositide phospholipase C by the actin-binding protein, profilin. *Plant J*. 6:389-400.

Eun, S.O., and Y. Lee. 1997. Actin filaments of guard cells are reorganized in response to light and abscisic acid. *Plant Physiol*. 115:1491-1498.

Feijo, J.A., J. Sainhas, T. Holdaway-Clarke, M.S. Cordeiro, J.G. Kunkel, and P.K. Hepler. 2001. Cellular oscillations and the regulation of growth: the pollen tube paradigm. *Bioessays*. 23:86-94.

Foote, H.C., J.P. Ride, V.E. Franklin-Tong, E.A. Walker, M.J. Lawrence, and F.C. Franklin. 1994. Cloning and expression of a distinctive class of self-incompatibility (S) gene from *Papaver rhoeas* L. *Proc Natl Acad Sci U S A*. 91:2265-2269.

Franklin-Tong, V.E., B.K. Drobak, A.C. Allan, P. Watkins, and A.J. Trewavas. 1996. Growth of Pollen Tubes of *Papaver rhoeas* Is Regulated by a Slow-Moving Calcium Wave Propagated by Inositol 1,4,5-Trisphosphate. *Plant Cell*. 8:1305-1321.

Franklin-Tong, V.E., G. Hackett, and P.K. Hepler. 1997. Ratio-imaging of Ca^{2+I} in the self-incompatibility response in pollen tubes of *Papaer rhoeas*. *Plant J*. 12:13675-13686.

Franklin-Tong, V.E., J.P. Ride, N.D. Read, A.J. Trewavas, and F.C.H. Franklin. 1993. The Self-Incompatibility Response in *Papaver-Rhoeas* Is Mediated by Cytosolic-Free Calcium. *Plant J*. 4:163-177.

Fu, Y., G. Wu, and Z. Yang. 2001. Rop GTPase-dependent dynamics of tip-localized F-actin controls tip growth in pollen tubes. *J Cell Biol*. 152:1019-1032.

Gao, X.Q., J. Chen, P.C. Wei, F. Ren, and X.C. Wang. 2008. Array and distribution of actin filaments in guard cells contribute to the determination of stomatal aperture. *Plant Cell Rep*. 27:1655-1665.

Geitmann, A., B.N. Snowman, A.M. Emons, and V.E. Franklin-Tong. 2000. Alterations in the actin cytoskeleton of pollen tubes are induced by the self-incompatibility reaction in *Papaver rhoeas*. *Plant Cell*. 12:1239-1251.

Gibbon, B.C., D.R. Kovar, and C.J. Staiger. 1999. Latrunculin B has different effects on pollen germination and tube growth. *Plant Cell*. 11:2349-2363.

Gourlay, C.W., L.N. Carpp, P. Timpson, S.J. Winder, and K.R. Ayscough. 2004. A role for the actin cytoskeleton in cell death and aging in yeast. *J Cell Biol*. 164:803-809.

Gungabissoon, R.A., C.-J. Jiang, B.K. Drøbak, S.K. Maciver, and P.J. Hussey. 1998. Interaction of maize actin-depolymerising factor with actin and phosphoinositides and its inhibition of plant phospholipase C. *Plant J*. 16:689-696.

Hepler, P.K., L. Vidali, and A.Y. Cheung. 2001. Polarized cell growth in higher plants. *Annu Rev Cell Dev Biol*. 17:159-187.

Higaki, T., N. Kutsuna, T. Sano, N. Kondo, and S. Hasezawa. 2010. Quantification and cluster analysis of actin cytoskeletal structures in plant cells: role of actin bundling in stomatal movement during diurnal cycles in *Arabidopsis* guard cells. *Plant J*. 61:156-165.

Holdaway-Clarke, T.L., and P.K. Hepler. 2003. Control of pollen tube growth: role of ion gradients and fluxes. *New Phytol*. 159:539-563.

Honys, D., and D. Twell. 2003. Comparative analysis of the *Arabidopsis* pollen transcriptome. *Plant Physiol*. 132:640-652.

Huang, S., L. Blanchoin, F. Chaudhry, V.E. Franklin-Tong, and C.J. Staiger. 2004. A gelsolin-like protein from *Papaver rhoeas* pollen (PrABP80) stimulates calcium-regulated severing and depolymerization of actin filaments. *J Biol Chem*. 279:23364-23375.

Huang, S., L. Blanchoin, D.R. Kovar, and C.J. Staiger. 2003. *Arabidopsis* capping protein (AtCP) is a heterodimer that regulates assembly at the barbed ends of actin filaments. *J Biol Chem*. 278:44832-44842.

Huang, S., X. Qu, and R. Zhang. 2015. Plant villins: versatile actin regulatory proteins. *J Integr Plant Biol*. 57:40-49.

Huang, S., R.C. Robinson, L.Y. Gao, T. Matsumoto, A. Brunet, L. Blanchoin, and C.J. Staiger. 2005. *Arabidopsis* VILLIN1 generates actin filament cables that are resistant to depolymerization. *Plant Cell*. 17:486-501.

Hussey, P.J., T. Ketelaar, and M.J. Deeks. 2006. Control of the actin cytoskeleton in plant cell growth. *Annu Rev Plant Biol*. 57:109-125.

Hwang, J.U., Y. Gu, Y.J. Lee, and Z. Yang. 2005. Oscillatory ROP GTPase activation leads the oscillatory polarized growth of pollen tubes. *Mol Biol Cell*. 16:5385-5399.

Hwang, J.U., and Y. Lee. 2001. Abscisic acid-induced actin reorganization in guard cells of dayflower is mediated by cytosolic calcium levels and by protein kinase and protein phosphatase activities. *Plant Physiol*. 125:2120-2128.

Janmey, P.A., K. Iida, H.L. Yin, and T.P. Stossel. 1987. Polyphosphoinositide micelles and polyphosphoinositide-containing vesicles dissociate endogenous gelsolin-actin complexes and promote actin assembly from the fast-growing end of actin filaments blocked by gelsolin. *J Biol Chem*. 262:12228-12236.

Jiang, Y., and S. Huang. 2017. Direct Visualization and Quantification of the Actin Nucleation and Elongation Events in vitro by TIRF Microscopy. *Bio Protoc*. 7:e2146.

Khurana, P., J.L. Henty, S. Huang, A.M. Staiger, L. Blanchoin, and C.J. Staiger. 2010. *Arabidopsis* VILLIN1 and VILLIN3 have overlapping and distinct activities in actin bundle formation and turnover. *Plant Cell*. 22:2727-2748.

Khurana, S., M. Arpin, R. Patterson, and M. Donowitz. 1997. Ileal microvillar protein villin is tyrosine-phosphorylated and associates with PLC-gamma1. Role of cytoskeletal rearrangement in the carbachol-induced inhibition of ileal NaCl absorption. *J Biol Chem*. 272:30115-30121.

Klahre, U., E. Friederich, B. Kost, D. Louvard, and N.H. Chua. 2000. Villin-like actin-binding proteins are expressed ubiquitously in *Arabidopsis*. *Plant Physiol*. 122:35-48.

Kovar, D.R., B.K. Drobak, and C.J. Staiger. 2000a. Maize profilin isoforms are functionally distinct. *Plant Cell*. 12:583-598.

Kovar, D.R., C.J. Staiger, E.A. Weaver, and D.W. McCurdy. 2000b. AtFim1 is an actin filament crosslinking protein from *Arabidopsis thaliana*. *Plant J*. 24:625-636.

Kuhn, J.R., and T.D. Pollard. 2005. Real-time measurements of actin filament polymerization by total internal reflection fluorescence microscopy. *Biophys J*. 88:1387-1402.

Kumar, N., A. Tomar, A.L. Parrill, and S. Khurana. 2004. Functional dissection and molecular characterization of calcium-sensitive actin-capping and actin-depolymerizing sites in villin. *J Biol Chem*. 279:45036-45046.

Li, J., L. Blanchoin, and C.J. Staiger. 2015. Signaling to actin stochastic dynamics. *Annu Rev Plant Biol*. 66:415-440.

Lin, Z., D.J. Eaves, E. Sanchez-Moran, F.C. Franklin, and V.E. Franklin-Tong. 2015. The *Papaver rhoeas* S determinants confer self-incompatibility to Arabidopsis thaliana in planta. *Science*. 350:684-687.

Livak, K.J., and T.D. Schmittgen. 2001. Analysis of relative gene expression data using real-time quantitative PCR and the 2(T)(-Delta Delta C) method. *Methods*. 25:402-408.

Maciver, S.K., and P.J. Hussey. 2002. The ADF/cofilin family: actin-remodeling proteins. *Genome Biol*. 3:reviews3007.

Markus, M.A., P. Matsudaira, and G. Wagner. 1997. Refined structure of villin 14T and a detailed comparison with other actin-severing domains. *Protein Sci*. 6:1197-1209.

McCurdy, D.W., D.R. Kovar, and C.J. Staiger. 2001. Actin and actin-binding proteins in higher plants. *Protoplasma*. 215:89-104.

Messerli, M., and K.R. Robinson. 1997. Tip localized Ca^{2+} pulses are coincident with peak pulsatile growth rates in pollen tubes of *Lilium longiflorum*. *J Cell Sci*. 110 (Pt 11):1269-1278.

Pierson, E.S., D.D. Miller, D.A. Callaham, A.M. Shipley, B.A. Rivers, M. Cresti, and P.K. Hepler. 1994. Pollen tube growth is coupled to the extracellular calcium ion flux and the intracellular calcium gradient: effect of BAPTA-type buffers and hypertonic media. *Plant Cell*. 6:1815-1828.

Pina, C., F. Pinto, J.A. Feijo, and J.D. Becker. 2005. Gene family analysis of the *Arabidopsis* pollen transcriptome reveals biological implications for cell growth, division control, and gene expression regulation. *Plant Physiol*. 138:744-756.

Pollard, T.D. 1984. Polymerization of ADP-actin. *J Cell Biol*. 99:769-777.

Pollard, T.D. 2016. Actin and Actin-Binding Proteins. *Cold Spring Harb Perspect Biol*. 8.

Poulter, N.S., M. Bosch, and V.E. Franklin-Tong. 2011. Proteins implicated in mediating self-incompatibility-induced alterations to the actin cytoskeleton of *Papaver* pollen. *Ann Bot*. 108:659-675.

Poulter, N.S., C.J. Staiger, J.Z. Rappoport, and V.E. Franklin-Tong. 2010. Actin-binding proteins implicated in the formation of the punctate actin foci stimulated by the self-incompatibility response in *Papaver*. *Plant Physiol*. 152:1274-1283.

Qu, X., H. Zhang, Y. Xie, J. Wang, N. Chen, and S. Huang. 2013. *Arabidopsis* villins promote actin turnover at pollen tube tips and facilitate the construction of actin collars. *Plant Cell*. 25:1803-1817.

Qu, X., R. Zhang, M. Zhang, M. Diao, Y. Xue, and S. Huang. 2017. Organizational Innovation of Apical Actin Filaments Drives Rapid Pollen Tube Growth and Turning. *Mol Plant*. 10:930-947.

Revenu, C., M. Courtois, A. Michelot, C. Sykes, D. Louvard, and S. Robine. 2007. Villin severing activity enhances actin-based motility in vivo. *Mol Biol Cell*. 18:827-838.

Rudd, J.J., and V.E. Franklin-Tong. 2003. Signals and targets of the self-incompatibility response in pollen of *Papaver rhoeas*. *J Exp Bot*. 54:141-148.

Sano, T., T. Higaki, Y. Oda, T. Hayashi, and S. Hasezawa. 2005. Appearance of actin microfilament 'twin peaks' in mitosis and their function in cell plate formation, as visualized in tobacco BY-2 cells expressing GFP-fimbrin. *Plant J*. 44:595-605.

Shi, M., Y. Xie, Y. Zheng, J. Wang, Y. Su, Q. Yang, and S. Huang. 2013. *Oryza sativa* actin-interacting protein 1 is required for rice growth by promoting actin turnover. *Plant J*. 73:747-760.

Smith, L.G., and D.G. Oppenheimer. 2005. Spatial control of cell expansion by the plant cytoskeleton. *Annu Rev Cell Dev Biol*. 21:271-295.

Snowman, B.N., D.R. Kovar, G. Shevchenko, V.E. Franklin-Tong, and C.J. Staiger. 2002. Signal-mediated depolymerization of actin in pollen during the self-incompatibility response. *Plant Cell*. 14:2613-2626.

Spudich, J.A., and S. Watt. 1971. The regulation of rabbit skeletal muscle contraction. I. Biochemical studies of the interaction of the tropomyosin-troponin complex with actin and the proteolytic fragments of myosin. *J Biol Chem*. 246:4866-4871.

Staiger, C.J. 2000. Signaling to the Actin Cytoskeleton in Plants. *Annu Rev Plant Physiol Plant Mol Biol*. 51:257-288.

Staiger, C.J., and V.E. Franklin-Tong. 2003. The actin cytoskeleton is a target of the self-incompatibility response in Papaver rhoeas. *J Exp Bot*. 54:103-113.

Takemoto, D., D.A. Jones, and A.R. Hardham. 2003. GFP-tagging of cell components reveals the dynamics of subcellular re-organization in response to infection of *Arabidopsis* by oomycete pathogens. *Plant J*. 33:775-792.

Thomas, S.G., S. Huang, S. Li, C.J. Staiger, and V.E. Franklin-Tong. 2006. Actin depolymerization is sufficient to induce programmed cell death in self-incompatible pollen. *J Cell Biol*. 174:221-229.

van der Honing, H.S., H. Kieft, A.M. Emons, and T. Ketelaar. 2012. *Arabidopsis* VILLIN2 and VILLIN3 are required for the generation of thick actin filament bundles and for directional organ growth. *Plant Physiol*. 158:1426-1438.

Vidali, L., and P.K. Hepler. 1997. Characterization and localization of profilin in pollen grains and tubes of *Lilium longiflorum*. *Cell Motil Cytoskeleton*. 36:323-338.

Vidali, L., S.T. McKenna, and P.K. Hepler. 2001. Actin polymerization is essential for pollen tube growth. *Mol Biol Cell*. 12:2534-2545.

Wang, L., Z. Lin, M. Trivino, M.K. Nowack, V.E. Franklin-Tong, and M. Bosch. 2019. Self-incompatibility in *Papaver* pollen: programmed cell death in an acidic environment. *J Exp Bot*. 70:2113-2123.

Wheeler, M.J., S. Vatovec, and V.E. Franklin-Tong. 2010. The pollen S-determinant in *Papaver*: comparisons with known plant receptors and protein ligand partners. *J Exp Bot*. 61:2015-2025.

Wilkins, K.A., J. Bancroft, M. Bosch, J. Ings, N. Smirnoff, and V.E. Franklin-Tong. 2011. Reactive oxygen species and nitric oxide mediate actin reorganization and programmed cell death in the self-incompatibility response of papaver. *Plant Physiol*. 156:404-416.

Wilkins, K.A., M. Bosch, T. Haque, N. Teng, N.S. Poulter, and V.E. Franklin-Tong. 2015. Self-incompatibility-induced programmed cell death in field poppy pollen involves dramatic acidification of the incompatible pollen tube cytosol. *Plant Physiol*. 167:766-779.

Wilkins, K.A., N.S. Poulter, and V.E. Franklin-Tong. 2014. Taking one for the team: self-recognition and cell suicide in pollen. *J Exp Bot*. 65:1331-1342.

Wu, J., S. Wang, Y. Gu, S. Zhang, S.J. Publicover, and V.E. Franklin-Tong. 2011. Self-incompatibility in Papaver rhoeas activates nonspecific cation conductance permeable to Ca^{2+} and K^{+}. *Plant Physiol*. 155:963-973.

Wu, S., Y. Xie, J. Zhang, Y. Ren, X. Zhang, J. Wang, X. Guo, F. Wu, P. Sheng, J. Wang, C. Wu, H. Wang, S. Huang, and J. Wan. 2015. VLN2 Regulates Plant Architecture by Affecting Microfilament Dynamics and Polar Auxin Transport in Rice. *Plant Cell*. 27:2829-2845.

Wu, Y., J. Yan, R. Zhang, X. Qu, S. Ren, N. Chen, and S. Huang. 2010. *Arabidopsis* FIMBRIN5, an actin bundling factor, is required for pollen germination and pollen tube growth. *Plant Cell*. 22:3745-3763.

Ye, J., Y. Zheng, A. Yan, N. Chen, Z. Wang, S. Huang, and Z. Yang. 2009. *Arabidopsis* formin3 directs the formation of actin cables and polarized growth in pollen tubes. *Plant Cell*. 21:3868-3884.

Yokota, E., and T. Shimmen. 1999. The 135-kDa actin-bundling protein from lily pollen tubes arranges F-actin into bundles with uniform polarity. *Planta*. 209:264-266.

Yokota, E., M. Tominaga, I. Mabuchi, Y. Tsuji, C.J. Staiger, K. Oiwa, and T. Shimmen. 2005. Plant villin, lily P-135-ABP, possesses G-actin binding activity and accelerates the polymerization and depolymerization of actin in a Ca2+-sensitive manner. *Plant Cell Physiol*. 46:1690-1703.

Yokota, E., L. Vidali, M. Tominaga, H. Tahara, H. Orii, Y. Morizane, P.K. Hepler, and T. Shimmen. 2003. Plant 115-kDa actin-filament bundling protein, P-115-ABP, is a homologue of plant villin and is widely distributed in cells. *Plant Cell Physiol*. 44:1088-1099.

Yu, M.M., M. Yuan, and H.Y. Ren. 2006. Visualization of actin cytoskeletal dynamics during the cell cycle in tobacco (*Nicotiana tabacum* L. cv *Bright Yellow*) cells. *Biol Cell*. 98:295-306.

Zhai, L., P. Zhao, A. Panebra, A.L. Guerrerio, and S. Khurana. 2001. Tyrosine phosphorylation of villin regulates the organization of the actin cytoskeleton. *J Biol Chem*. 276:36163-36167.

Zhang, H., X. Qu, C. Bao, P. Khurana, Q. Wang, Y. Xie, Y. Zheng, N. Chen, L. Blanchoin, C.J. Staiger, and S. Huang. 2010. *Arabidopsis* VILLIN5, an actin filament bundling and severing protein, is necessary for normal pollen tube growth. *Plant Cell*. 22:2749-2767.

Zhang, R., M. Chang, M. Zhang, Y. Wu, X. Qu, and S. Huang. 2016. The Structurally Plastic CH2 Domain Is Linked to Distinct Functions of Fimbrins/Plastins. *J Biol Chem*. 291:17881-17896.

Zhang, R.H., X.L. Qu, M. Zhang, Y.X. Jiang, A.B. Dai, W.Y. Zhao, D. Cao, Y.X. Lan, R. Yu, H.W. Wang, and S.J. Huang. 2019. The Balance between Actin-Bundling Factors Controls Actin Architecture in Pollen Tubes. *Iscience*. 16:162-+.

Zhang, Y., Y. Xiao, F. Du, L. Cao, H. Dong, and H. Ren. 2011. Arabidopsis VILLIN4 is involved in root hair growth through regulating actin organization in a Ca^{2+}-dependent manner. *New Phytol*. 190:667-682.

Figures

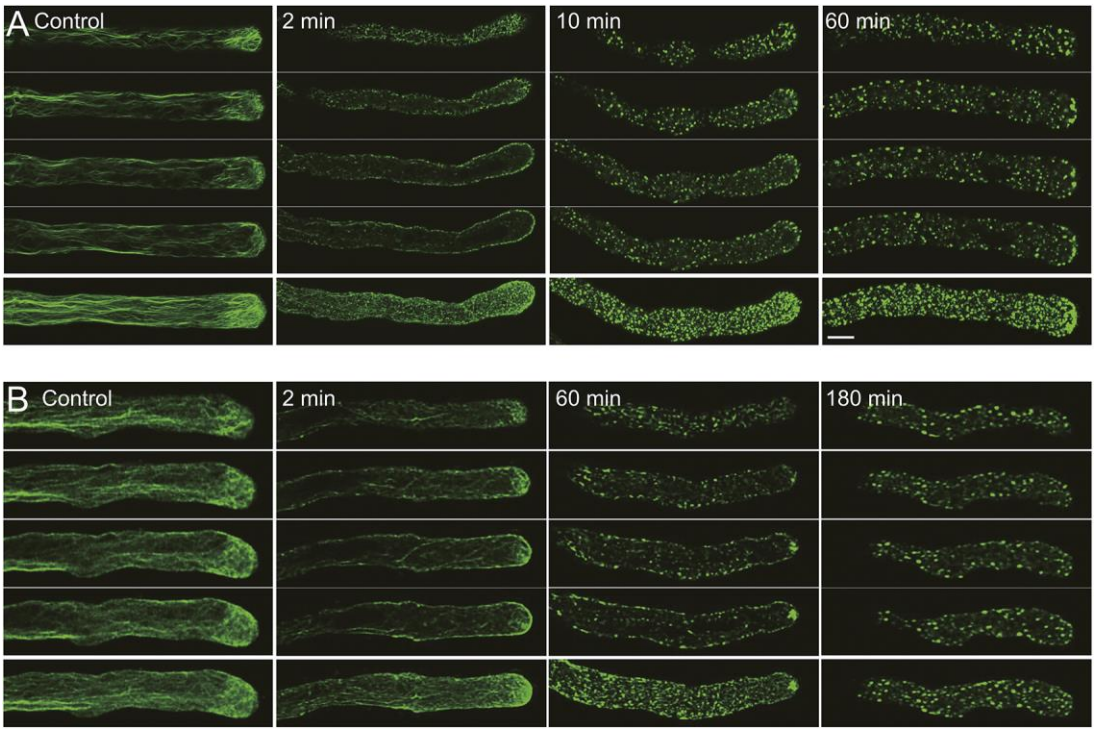

Figure 1. A23187 Treatment Triggers similar Actin Alterations in *Arabidopsis* Pollen Tubes to that of SI Pollen Tubes

(**A**) Confocal images of actin filaments in WT *Arabidopsis thaliana* pollen tubes treated with 10 μM A23187. Treatment with 10 μM A23187 allows us to see the alterations and difference in the actin cytoskeleton in pollen tubes during treatment. Actin filaments were stained with Alexa-488-phalloidin. Images of actin filaments in pollen tubes after the treatment with A23187 at different time points are presented. The bottom row shows full projections; the rows above show the associated optical sections. Bar = 10 μm for (**A**) and (**B**).

(**B**) Confocal images of actin filaments in *Arabidopsis* pollen tubes expressing $PrpS_1$ (*At-ntp303p::PrpS*$_1$*-GFP*) after SI induction. SI responses were triggered by the treatment with 20 ng.μl^{-1} recombinant $PrsS_1$. F-actin was stained with rhodamine phalloidin. F-actin in pollen tubes during the SI response at different time points are shown. The bottom row shows full projections; the rows above show the associated optical sections. Note that the actin remodelling, though very similar, is slower than the response to A23187.

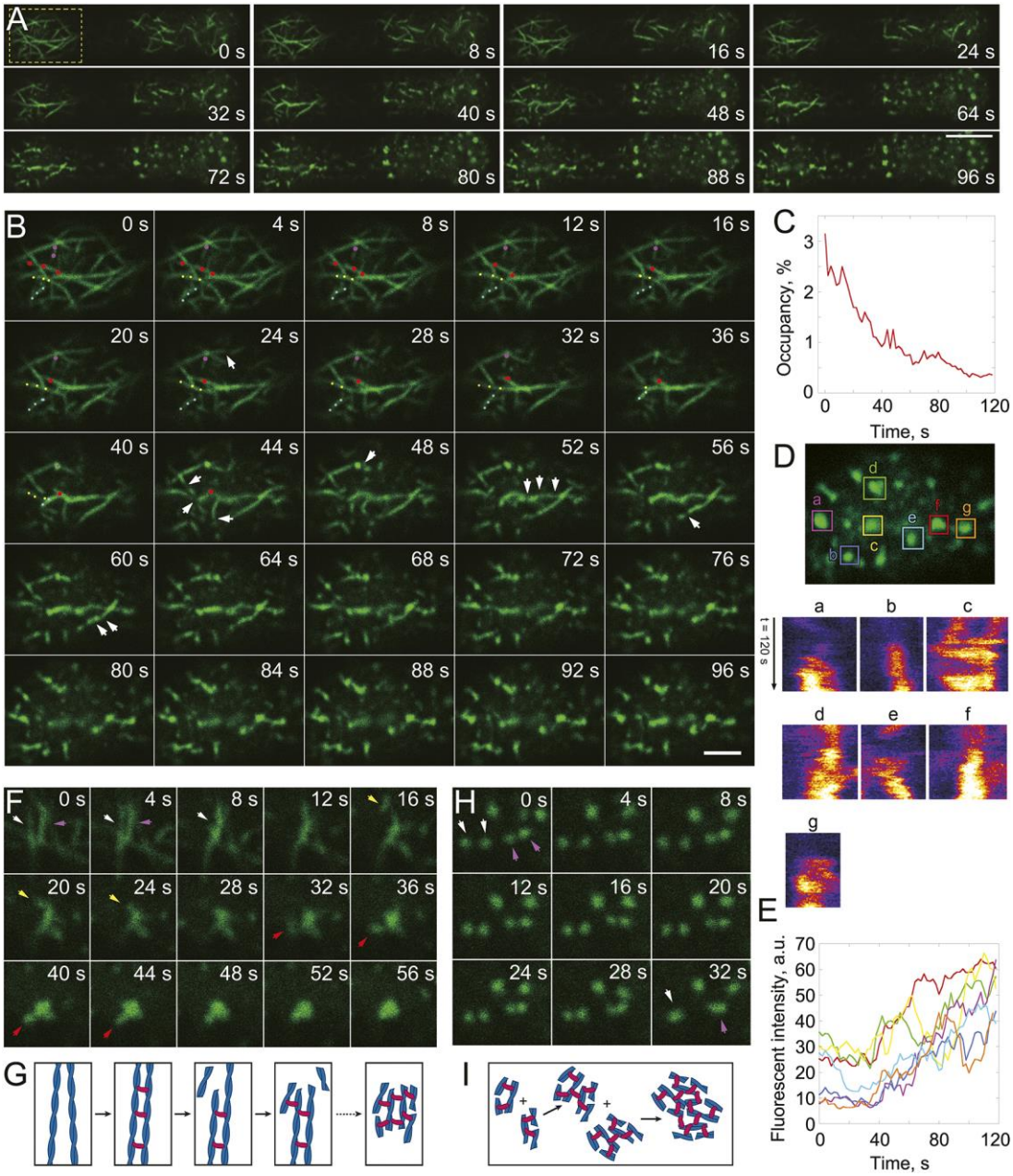

Figure 2. A23187 Treatment Induces Rearrangement, Fragmentation and Depolymerization of Actin Filaments as well as the Formation and Subsequent Enlargement of Actin Foci in Pollen Tubes

(**A**) Time-series images of actin filaments in a living WT pollen tube expressing Lifeact-EGFP treated with 10 μM A23187. Actin filaments were revealed by decoration with Lifeact-EGFP. Bar = 10 μm. t = 0 represents the time point when the movie recording started, immediately after treatment.

(**B**) Time-series images of actin filaments within the boxed region shown in (**A**). The

red, pink, blue and yellow dots mark different actin filaments, which underwent apparent depolymerization during A23187 treatment. The white arrows indicate actin filament fragmentation events. Bar = 2 μm.

(**C**) Quantification of the "occupancy" of actin filaments in pollen tubes. The occupancy of actin filaments was plotted versus the time after A23187 addition.

(**D**) Kymographs of actin foci during A23187 treatment. The upper panel shows the actin foci of interest traced for kymograph analysis in the lower panels and the measurement of the fluorescence intensity in (**E**) (indicated by different colored boxes).

(**E**) Quantification of the fluorescence intensity of actin foci. For time points prior to the formation of foci, the fluorescence intensity of actin filaments at the location where foci subsequently formed was measured. The plot shows that the fluorescence intensity of these actin foci increasing over time.

(**F**) Time-lapse images of actin filaments showing the formation and enlargement of actin foci. Red, white, yellow and purple arrowheads indicate actin filament fragments that appeared to aggregate/fuse with other actin fragments.

(**G**) Schematic describing the formation of the actin foci by aggregation/fusion. Actin filaments (indicated in blue) were first bundled and then fragmented into short fragments. These short actin fragments aggregated/fused together via the action of villin (indicated in red), while simultaneously being further fragmented and shortened, until they formed larger punctate foci.

(**H**) Time-lapse images showing the formation of actin foci. White and pink arrows at 0 s indicate actin foci before crosslinking; white and pink arrows at 32 s indicate actin foci after crosslinking.

(**I**) Schematic describing the enlargement of actin foci by the crosslinking of small actin foci. Fragmented actin filament bundles (indicated in blue) crosslinked by villin (indicated in red) were fragmented; these were further fragmented, shortened and cross-linked, until they formed larger punctate foci.

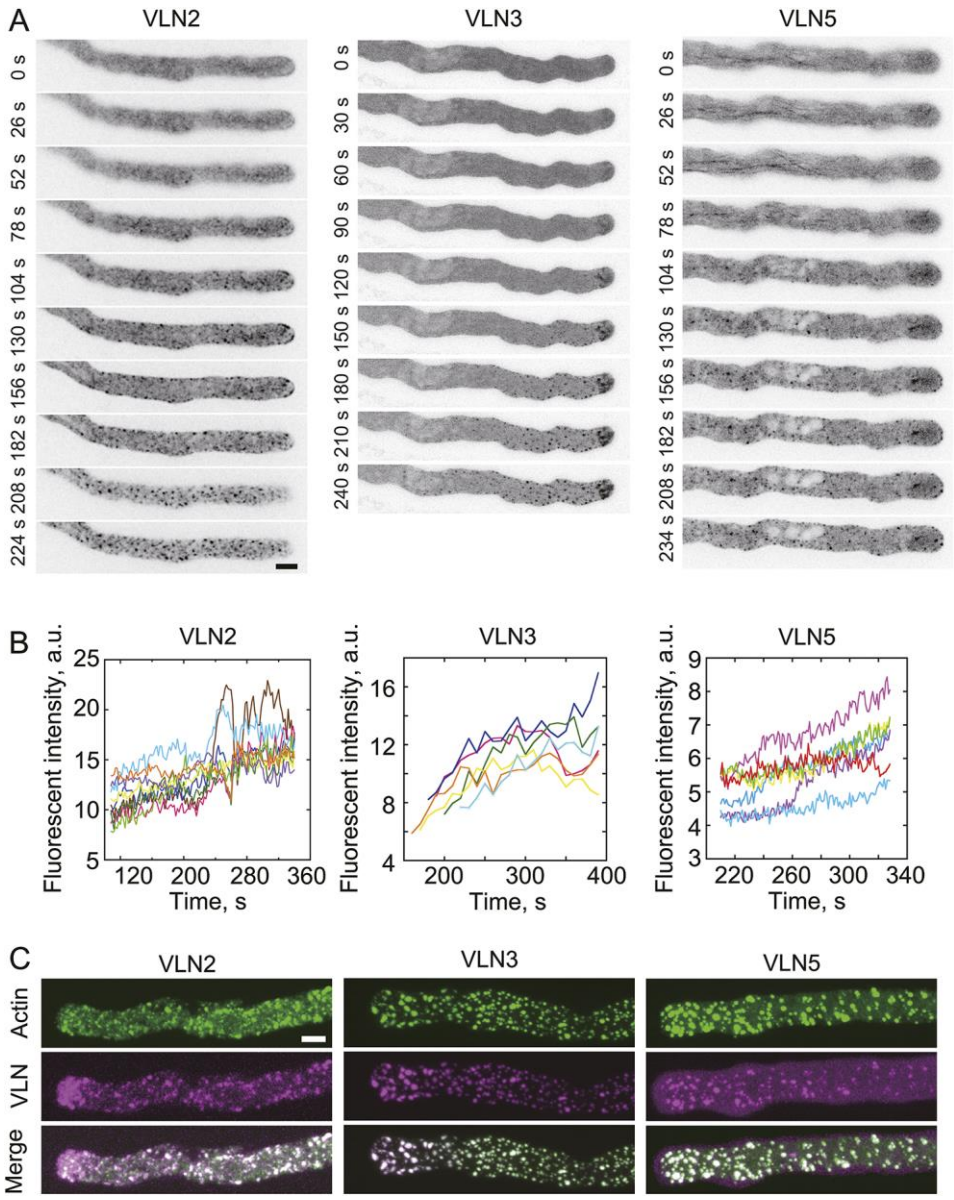

Figure 3. VLN2, VLN3 and VLN5 Colocalize with Actin Foci in Pollen Tubes

(**A**) Time series of images showing the localization of VLN2, VLN3 and VLN5 (seen as black dots) in pollen tubes during treatment with A23187. Pollen tubes from lines *VLN2pro:VLN2-EGFP;vln2*, *VLN3pro:VLN3-EGFP;vln3* and *VLN5pro:VLN5-EGFP;vln5* were subjected to treatment with A23187 when their average length reached about 150 μm. Bar = 5 μm.

(**B**) Quantification of the fluorescence intensity of dots formed by VLN2-EGFP, VLN3-EGFP or VLN5-EGFP showing an increase over time. The fluorescence intensity of dots was plotted versus time. VLN2, n = 9, VLN3, n = 6, VLN4, n = 7.

(**C**) Images showing colocalization of VLN-GFP fusion proteins with actin after treatment with 50 μM A23187 for 60 min. Treatment with 50 μM A23187 was performed in order to see the formation of obvious F-actin foci in pollen tubes. F-actin foci were stained with Alexa-568-phalloidin. Bar = 5 μm.

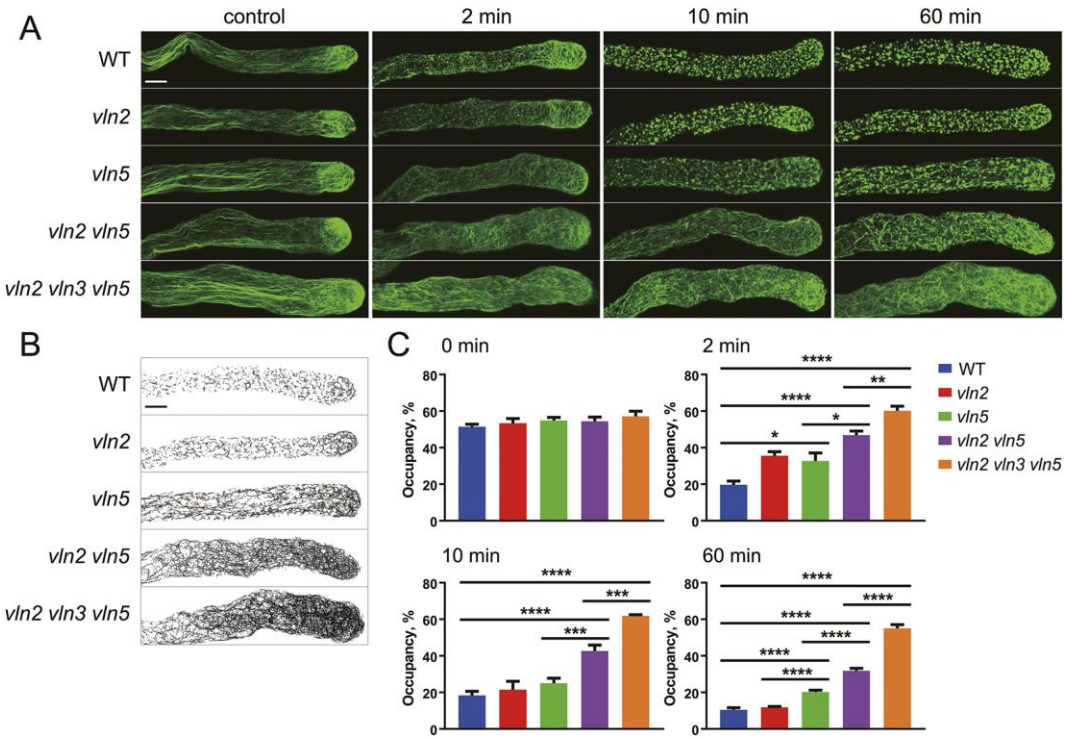

Figure 4. Loss of Function of *Arabidopsis VLNs* Impair the Depolymerization of Actin Filaments and the Formation of Actin Foci in Response to A23187 Treatment in Pollen Tubes

(**A**) F-actin in pollen tubes visualized by staining with Alexa-488 phalloidin and confocal imaging. Pollen tubes from various lines: WT, *vln2*, *vln5*, *vln2 vln5* and *vln2 vln3 vln5* mutants were treated with 10 μM A23187 for 2 min, 10 min and 60 min. While on their own, the mutants had a relatively small effect on actin configuration, the double and triple mutants had much larger impact. Bar = 5 μm.

(**B**) Skeletonized images of actin filaments in WT, *vln2*, *vln5*, *vln2 vln5* and *vln2 vln3 vln5* mutant pollen tubes after treatment with 10 μM A23187 for 60 min show clear differences between the amount of actin filaments in different mutant lines. Bar = 5 μm.

(**C**) Quantification of the occupancy of actin filaments in WT and *villin* mutant pollen tubes after treatment with A23187. The occupancy of actin filaments in WT and *villin* mutant pollen tubes was plotted, showing significant differences between these. Values represent mean ± SE, n > 8, *P < 0.05, **P < 0.01, ***P < 0.001, ****P < 0.0001, by student's t-test.

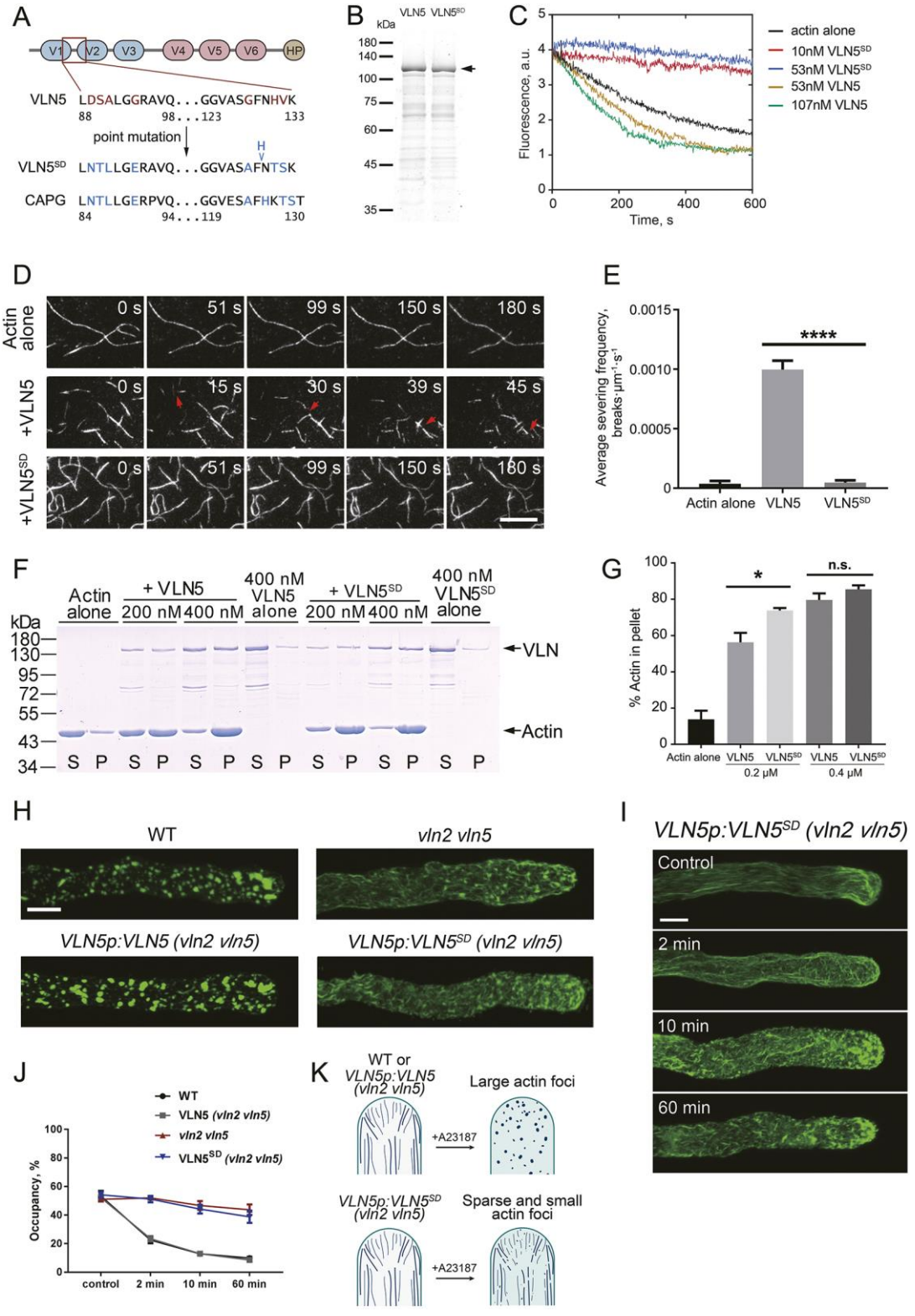

Figure 5. The Severing Activity of VLN5 is required for A23187-induced Fragmentation and Depolymerization of Actin Filaments and the Formation of Actin Foci in Pollen Tubes

(**A**) A cartoon describing the severing deficient VLN5 protein $VLN5^{SD}$ generated according to (Revenu et al., 2007). A series of mutations, located in the boxed region, were introduced into VLN5 via comparison with CapG, as this region was shown to be crucial for the severing activity of villin. The amino acid sequences of VLN5, $VLN5^{SD}$ and CapG are shown. The mutated sequences in VLN5 are brown colored, and the corresponding sequences in CapG are light blue colored. Besides the point mutations, a histidine was inserted in $VLN5^{SD}$.

(**B**) SDS-PAGE analysis of purified recombinant VLN5 and $VLN5^{SD}$ proteins. Arrow indicates recombinant VLN5 and $VLN5^{SD}$.

(**C**) $VLN5^{SD}$ prevents whereas VLN5 enhances dilution-mediated actin depolymerization, suggesting that the severing activity of $VLN5^{SD}$ was impaired. Preassembled actin filaments at 5 μM (50% pyrene-labeled) were diluted 25-fold in G buffer in the presence of 0.2 mM free Ca^{2+}. The decrease in pyrene fluorescence accompanying actin depolymerization was monitored over time. The two concentrations of $VLN5^{SD}$ mutant show lack of actin depolymerization.

(**D**) Time-lapse images of actin filaments visualized by TIRFM. Red arrows indicate the fragmentation events of actin filaments. Bars = 5 μm.

(**E**) Quantification of actin filaments severing frequency. The severing frequency of $VLN5^{SD}$ is significantly lower than that of VLN5, suggesting that $VLN5^{SD}$ has decreased severing activity. Values represent mean ± SE, n = 45, ****P < 0.0001, by student's *t*-test.

(**F**) SDS-PAGE analysis of the protein samples from F-actin low-speed cosedimentation experiments. Equal volume of protein samples from the supernatant (S) and pellet (P) were separated by SDS-PAGE.

(**G**) Quantification of the amount of actin in the pellet fractions. There was no large difference in the amount of actin in the pellet fractions of samples containing VLN5^{SD} compared with samples containing VLN5, indicating that the bundling activity of VLN5^{SD} was not greatly impaired. Values represent mean ± SE, n = 3, *P < 0.05, by student's *t*-test. n.s., not significant.

(**H**) Images of actin filaments in pollen tubes. WT, *vln2 vln5* and VLN5^{SD} (*vln2 vln5*) pollen tubes were subjected to actin staining with Alexa-488 phalloidin after treatment with 50 μM A23187 for 60 min. Using 50 μM A23187 treatment allows the formation of obvious F-actin foci in WT pollen tubes. This shows that the VLN5 can rescue the defective actin reorganization found in *vln2 vln5* mutant pollen tubes and the VLN5^{SD} cannot do so. Bar = 5 μm.

(**I**) Images of actin filaments in the VLN5^{SD} (*vln2 vln5*) mutant at different time points after treated with 50 μM A23187. Bar = 5 μm.

(**J**) Quantification of the occupancy of actin filaments in pollen tubes after treatment with 10 μM A23187 showing that the VLN5^{SD} has a defective actin depolymerization response to A23187 similar to the *vln2 vln5* mutant. Values represent mean ± SE, n = 8.

(**K**) Schematic diagram showing the alteration in the organization of actin filaments in WT or V5p:VLN5 (*vln2 vln5*) and VLN5^{SD} (*vln2 vln5*) pollen tubes after the treatment with A23187. After A23187 treatment, in the WT or V5p:VLN5 (*vln2 vln5*) pollen tubes, actin filaments form large foci (upper panel). However, in the VLN5^{SD} (*vln2 vln5*) pollen tubes, after A23187 treatment, a much weaker response is detected and the actin foci are sparse and small.

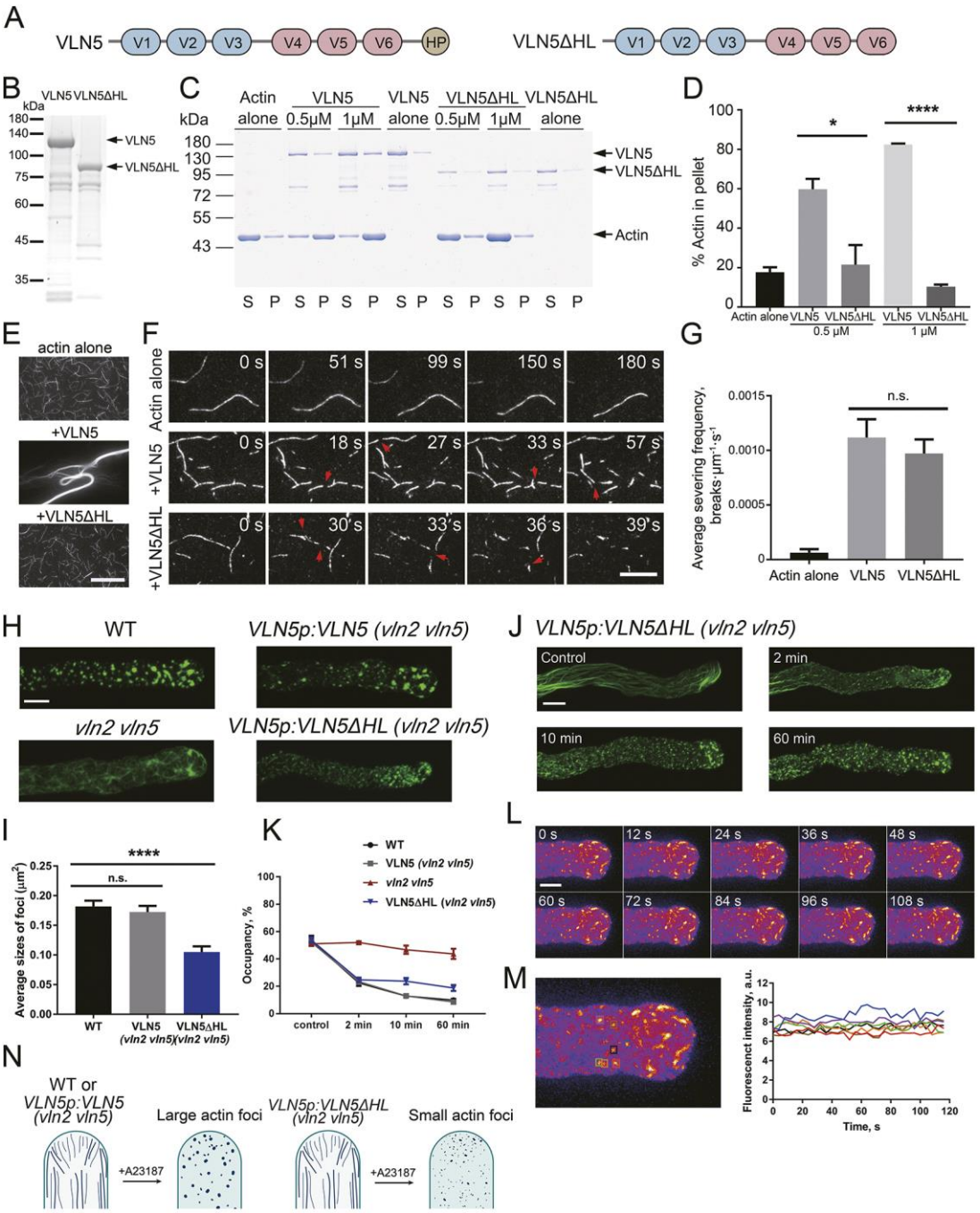

Figure 6. The Actin Bundling Activity of VLN5 is Required for the Enlargement of Actin Foci in Pollen Tubes

(**A**) A cartoon showing the generation of VLN5ΔHL protein, with deletion of the headpiece domain and the linker.

(**B**) SDS-PAGE analysis of purified recombinant VLN5 and VLN5ΔHL proteins. Arrow indicate the main bands of VLN5 and VLN5ΔHL.

(**C**) SDS-PAGE analysis of the protein samples from the low-speed F-actin cosedimentation experiment. S, supernatant; P, pellet.

(**D**) Quantification of the amount of actin in the pellet fractions. The amount of actin in pellet significantly decreased in samples with VLN5ΔHL, indicating that the bundling activity of VLN5ΔHL is impaired. Values represent mean ± SE, n = 3, *P < 0.05, ****P < 0.0001, by student's *t*-test.

(**E**) Images of F-actin stained with rhodamine phalloidin. F-actin, 2 μM; VLN5 or VLN5ΔHL, 0.5 μM. Bar = 20 μm.

(**F**) Time-lapse images of actin filaments captured by TIRFM. [VLN5] and [VLN5ΔHL], 3 nM; free [Ca^{2+}], 1.0 μM. Red arrowheads indicate the fragmentation events of actin filaments. Bar = 10 μm.

(**G**) Quantification of actin filament severing frequency. The severing frequency of VLN5ΔHL was not significantly different from that of VLN5, indicating that the severing activity of VLN5ΔHL remains unchanged. Data represent mean ± SE, n = 45, the statistical comparison was performed with Student's *t*-test. n.s., not significant.

(**H**) Images of actin filaments in WT, *vln2 vln5* and V5p:VLN5ΔHL (*vln2 vln5*) pollen tubes after treatment with 50 μM A23187 for 60 min and subsequently stained with Alexa488-phalloidin. Using the treatment with 50 μM A23187 enables the formation of obvious F-actin foci in pollen tubes at that time point. The actin foci formed in the VLN5p:VLN5ΔHL (*vln2 vln5*) pollen tubes were much reduced compared to those formed in the VLN5p:VLN5 (*vln2 vln5*) pollen tubes. Bar = 5 μm.

(**I**) Quantification of the size of actin foci in pollen tubes treated with 50 μM A23187. Values represent mean ± SE, n = 8. ****P < 0.0001, by student's *t*-test. n.s., not significant.

(**J**) Representative images of actin filaments stained with Alexa488-phalloidin in *VLN5p*:VLN5ΔHL (*vln2 vln5*) pollen tubes after treated with 10 μM A23187, showing an increase in fragmentation of actin structures in pollen tubes within 2 min and formation of punctate actin foci afterwards. Treatment with 10 μM A23187 was

performed in order to see the process of actin alterations in pollen tubes during treatment. Bar = 5 μm.

(**K**) Quantification of the occupancy of actin filaments in pollen tubes after treated with 10 μM A23187, showing that VLN5ΔHL pollen tubes could depolymerize actin filaments in response to A23187. Values represent mean ± SE, n = 8.

(**L**) Time-lapse images of VLN5ΔHL-mCherry in pollen tubes after treatment with A23187. Actin foci first formed at the pollen tube tip and then at sub-apical region after treatment with 10 μM A23187. t = 0 is the time point when foci were formed but not enlarged. Bar = 5 μm.

(**M**) Quantification of the fluorescence intensity of VLN5ΔHL-mCherry during the treatment with 10 μM A23187. The left panel shows the image of VLN5ΔHL-mCherry with the tracked dots indicated by different colored boxes. The right panel shows the plot of the fluorescence intensity of VLN5ΔHL-mCherry in the pollen tube over time in the presence of 10 μM A23187. These pollen tubes with the VLN5ΔHL did not make enlarged actin foci.

(**N**) Schematic description of the formation of actin foci in WT or V5p:VLN5 (*vln2 vln5*) and V5p:VLN5ΔHL (*vln2 vln5*) pollen tubes treated with A23187. After treatment with A23187, compared with WT or V5p:VLN5 (*vln2 vln5*) pollen tubes, which form large actin foci, the actin foci in V5p:VLN5ΔHL (*vln2 vln5*) pollen tubes failed to enlarge.

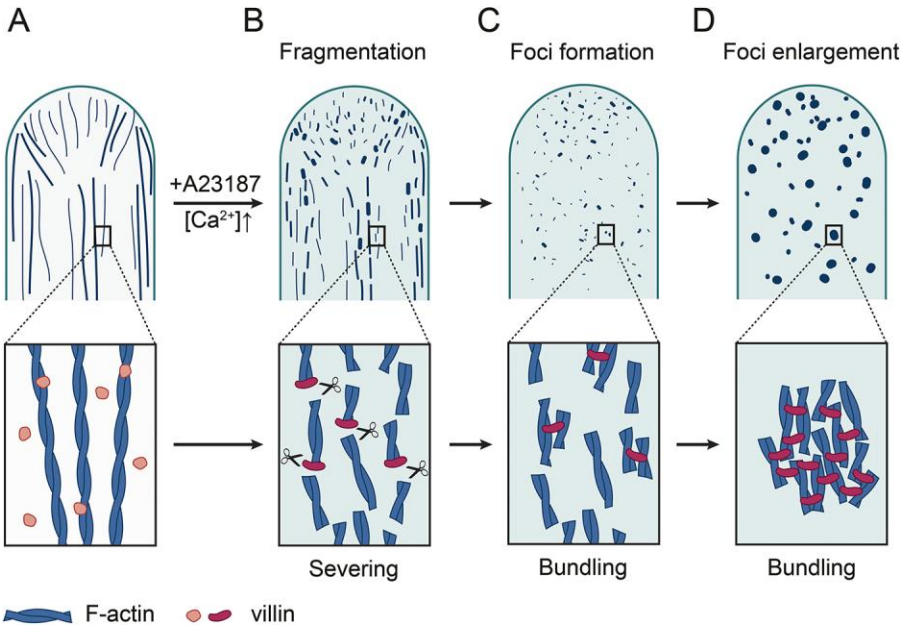

Figure 7. Schematic Model Describing Actin Alterations in Response to the A23187 treatment of Pollen Tubes, showing the Proposed Role of Villin

(**A**) In untreated growing pollen tube, actin filaments were organized in bundles.

(**B**) With the addition of A23187 (and assumed elevation of $[Ca^{2+}]_{cyt}$) in the pollen tube, the actin cytoskeleton starts to be broken down by the increase in the fragmentation of actin filaments. Villin is involved in fragmenting actin filaments by its Ca^{2+}–responsive actin severing activity. We assumed that the conformation of villin is altered after the addition of A23187.

(**C**) With prolonged treatment with A23187, actin filaments start to depolymerize. Villin facilitates this process by severing actin filaments. Meanwhile, actin foci start to form in the pollen tube. Villin is involved in foci formation by cross-linking actin fragments.

(**D**) The size of foci gradually increases over time. In this process, villin is involved in promoting the enlargement of actin foci via its actin bundling activity to link the fragmented actin structures together.

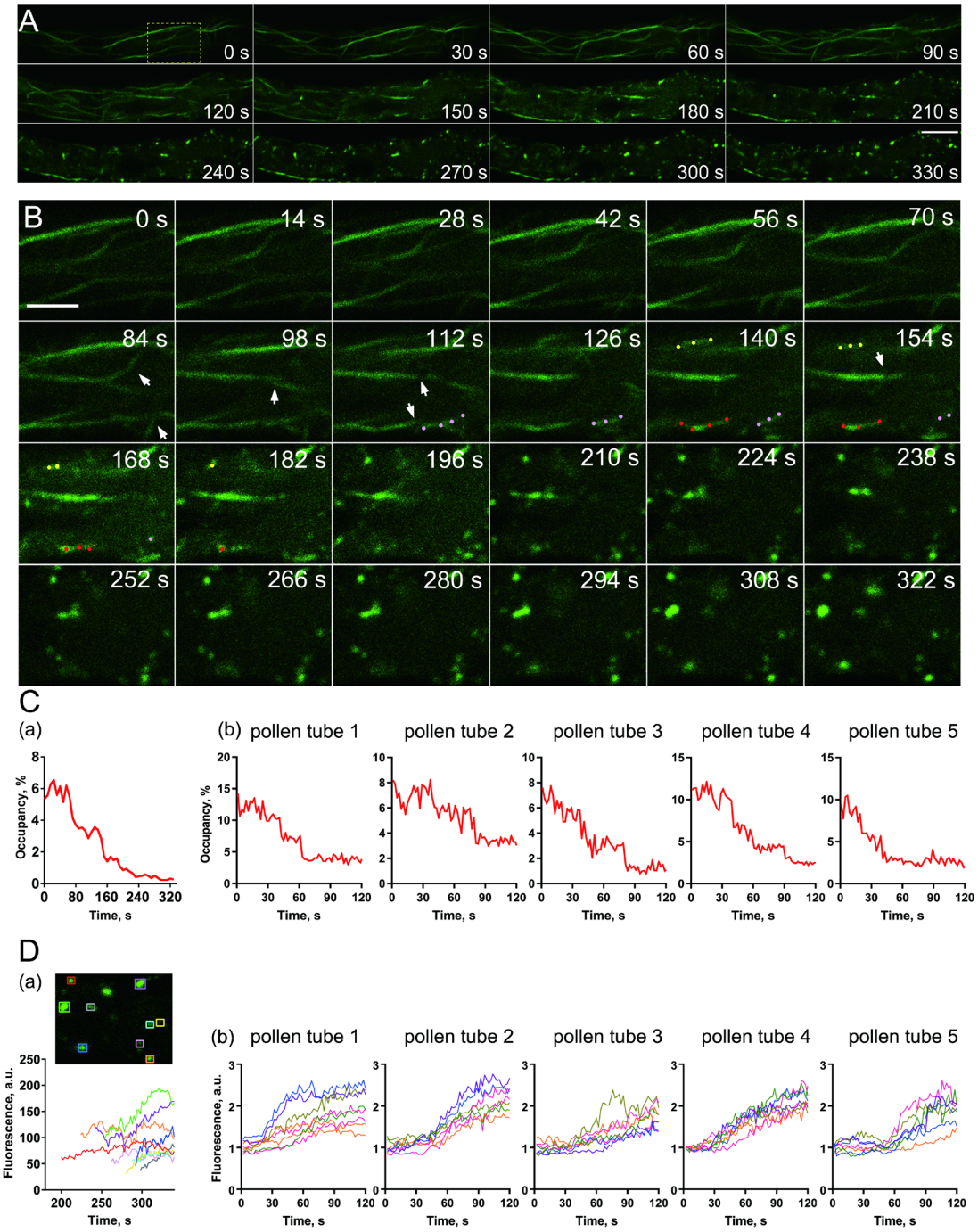

Figure S1. A23187 Treatment Induces Rearrangement, Fragmentation and Depolymerization of Actin Filaments as well as the Formation and Subsequent Enlargement of Actin Foci in Pollen Tubes

(**A**) Time-series of images showing remodeling of actin filaments in a living WT pollen tube expressing Lifeact-EGFP treated with 10 μM A23187. Actin filaments were revealed by decoration with Lifeact-EGFP. Bar = 5 μm. t = 0 represent the time

point when the rearrangement of actin filaments began.

(**B**) Time-series images of actin filaments within the boxed region shown in (**A**). The red, pink and yellow dots mark different actin filaments, which underwent apparent depolymerization during A23187 treatment. The white arrows indicate actin filament fragmentation events. Bar = 2 μm.

(**C**) Quantification of the occupancy of actin filaments in pollen tubes. (**a**) The occupancy of actin filaments was plotted versus the time after A23187 addition for the pollen tube shown in (**A**). (**b**) Plot of the occupancy of actin filaments versus the time after A23187 addition for 5 additional pollen tubes.

(**D**) Quantification of the fluorescence intensity of actin foci. (**a**) The upper panel shows the actin foci of interest traced for the measurement of the fluorescence intensity, which was indicated by different colored boxes. The lower panel shows the plot of fluorescence intensity of actin foci versus time; the fluorescence intensity of foci was recorded once the foci started to form. (**b**) Plots of fluorescence intensity of actin foci versus time for 5 additional pollen tubes.

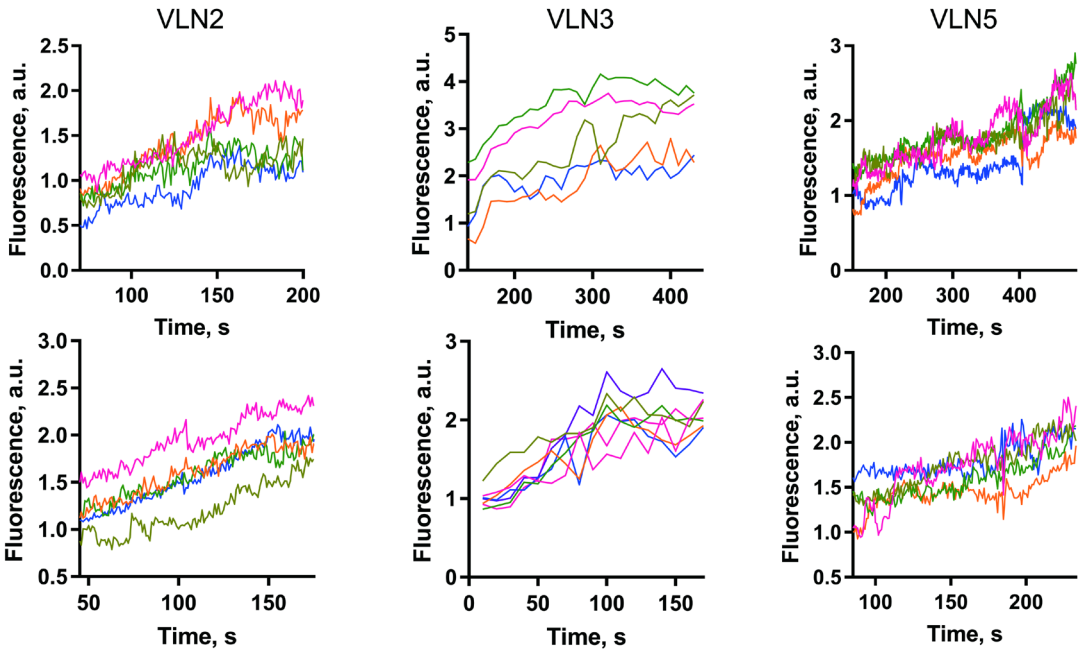

Figure S2. The Fluorescence Intensity of Actin Foci Decorated with VLN2-EGFP, VLN3-EGFP and VLN5-EGFP Increases Over Time

The fluorescence intensity of dots formed by VLN2-EGFP, VLN3-EGFP and VLN5-EGFP was measured in two pollen tubes for each GFP fusion protein, and was plotted versus time.

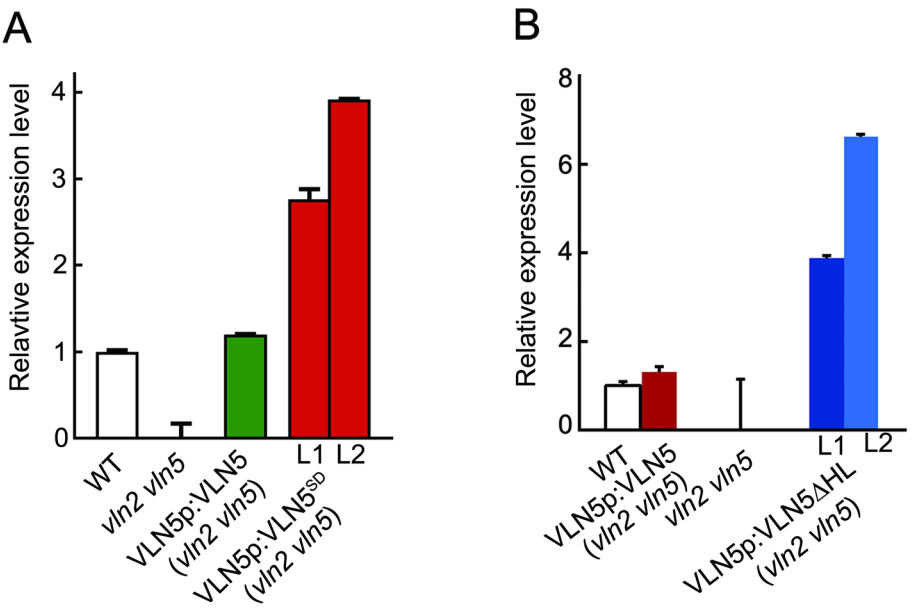

Figure S3. Determination of the Relative Amount of Transcripts of VLN5 and Its Variants in Pollen

(**A**) Analysis of the amount of *VLN5* transcripts in pollen. Pollen derived from WT, *vln2 vln5*, VLN5p:VLN5 (*vln2 vln5*), VLN5p:VLN5^{SD} (*vln2 vln5*) plants. VLN5p:VLN5 (*vln2 vln5*) are transgenic plant lines expressing *VLN5* under control of *VLN5* promoter in *vln2 vln5* double mutant.

(**B**) Analysis of the relative expression level of *VLN5* transcripts in pollen from various lines. Pollen was collected from WT, *vln2 vln5*, VLN5p:VLN5 (*vln2 vln5*), VLN5p:VLN5ΔHL (*vln2 vln5*) plants; see M&M for details.

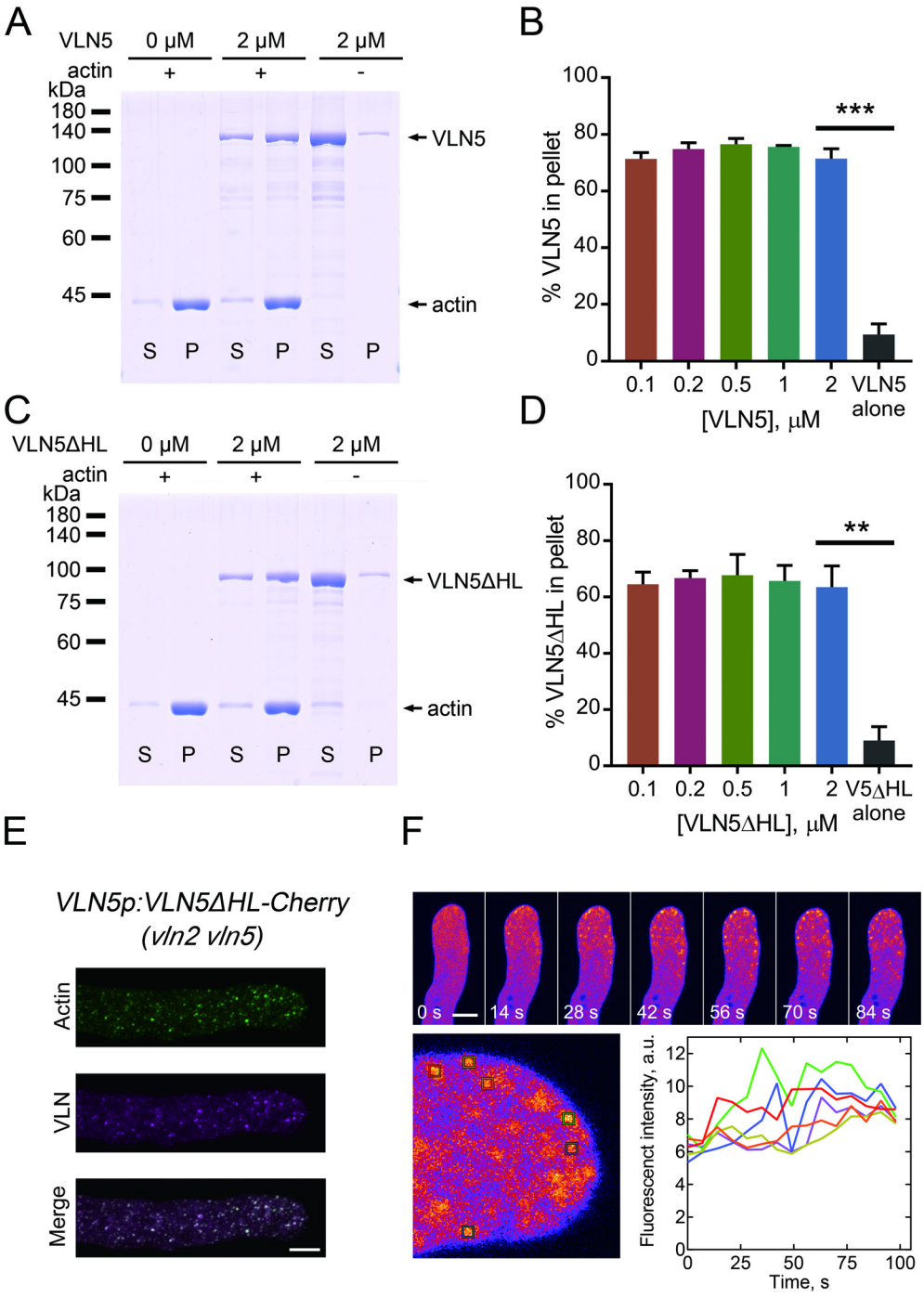

Figure S4. Actin Foci Decorated by VLN5ΔHL Fail to Enlarge

(**A**) SDS-PAGE analysis of the protein samples from the high-speed F-actin cosedimentation experiment. 2 μM of VLN5 (with 0 μM as control) was incubated with 3 μM F-actin for 30 min at room temperature before centrifugation. S, supernatant; P, pellet.

(**B**) Quantification of the amount of sedimented VLN5. The amount of VLN5 in pellet significantly increased after incubation with F-actin, indicating that VLN5 possesses F-actin binding ability. Values represent mean ± SE, n = 3. ***P < 0.001 by Student's t-test.

(**C**) SDS-PAGE analysis of the protein samples from the high-speed cosedimentation experiment. 2 μM of VLN5ΔHL (with 0 μM as control) was incubated with 3 μM F-actin for 30 min at room temperature before centrifugation. S, supernatant; P, pellet.

(**D**) Quantification of the amount of sedimented VLN5ΔHL. The amount of VLN5ΔHL in pellet significantly increased after incubation with F-actin, indicating that VLN5ΔHL possesses F-actin binding ability. Values represent mean ± SE, n = 3. **P<0.01, by Student's t-test.

(**E**) Images of actin and VLN5ΔHL-mCherry in *A. thaliana* pollen tubes after treated with A23187. Actin filaments were revealed by staining with Alexa-488 phalloidin. Actin foci and VLN5ΔHL-mCherry-decorated structures overlap substantially. Bar = 5 μm.

(**F**) Quantification of the dynamic behavior of VLN5ΔHL-mCherry in pollen tubes after treatment with A23187. The upper panel shows time-lapse images of VLN5ΔHL-mCherry in pollen tubes treated with 10 μM A23187. The lower panel shows the tracked VLN5ΔHL-mCherry dots (left) and quantification of their fluorescence intensities over time (right). Bar = 5 μm.

Supplemental Movies

Movie 1. Dynamic Behavior of Actin Filaments in Pollen Tube Treated with 10 μM A23187. Actin filaments decorated with Lifeact-EGFP were tracked after the treatment with 10 μM A23187. The movie is displayed at 5 frames per second.

Movie 2. Dynamic Formation of VLN2-EGFP Dots in a Pollen Tube after the Treatment with 10 μM A23187. VLN2-EGFP was tracked after the treatment with 10 μM A23187 showing the formation of dot-like structures. The movie is displayed at 5 frames per second.

Movie 3. Dynamic Formation of VLN3-EGFP Dots in a Pollen Tube after the Treatment with 10 μM A23187. VLN3-EGFP was tracked after the treatment with 10 μM A23187 showing the formation of dot-like structures. The movie is displayed at 2 frames per second.

Movie 4. Dynamic Formation of VLN5-EGFP Dots in a Pollen Tube after the Treatment with 10 μM A23187. VLN5-EGFP was tracked after the treatment with 10 μM A23187 showing the formation of dot-like structures. The movie is displayed at 5 frames per second.

Table 1. Primers used in this study

Primer name	Primer sequence
$VLN5CDS_F$	GGTACCGAGCTCCGATGACGTTTTCCATGAG
$VLN5CDS_R$	CTGCAGCTTCAGTTGCGCTC
$VLN5^{SD}{}_{1F}$	ACTATTAGGTGAACGTGCTGTTC
$VLN5^{SD}{}_{1R}$	GTATTTAAATCAACAGTCATGACGGC
$VLN5^{SD}{}_{2F}$	CACAACACTTCAAAGCCCGAGGA
$VLN5^{SD}{}_{2R}$	GAACGCTGAAGCAACTCCACCT
$VLN5\Delta HL_F$	GGTACCGAGCTCCGATGACGTTTTCCATGAGAGATTT
$VLN5\Delta HL_R$	GAATTCTTACTCGAGATTTGTCAGGATCGCAAGCTTTC
q*VLN5* F	TCGGTAAAGATTCCAGCCA
q*VLN5* R	GAACCCTGAAGCAACTCCAC